

# Discovery of ARD-1676 as a Highly Potent and Orally Efficacious AR PROTAC Degradator with a Broad Activity against AR Mutants for the Treatment of AR + Human Prostate Cancer

Weiguo Xiang,<sup>◆</sup> Lijie Zhao,<sup>◆</sup> Xin Han,<sup>◆</sup> Tianfeng Xu,<sup>◆</sup> Steven Kregel,<sup>◆</sup> Mi Wang,<sup>◆</sup> Bukeyan Miao, Chong Qin, Mingliang Wang, Donna McEachern, Jianfeng Lu, Longchuan Bai, Chao-Yie Yang, Paul D. Kirchhoff, John Takyi-Williams, Lu Wang, Bo Wen, Duxin Sun, Mark Ator, Robert Mckean, Arul M. Chinnaiyan, and Shaomeng Wang\*



Cite This: *J. Med. Chem.* 2023, 66, 13280–13303



Read Online

ACCESS |



Metrics & More



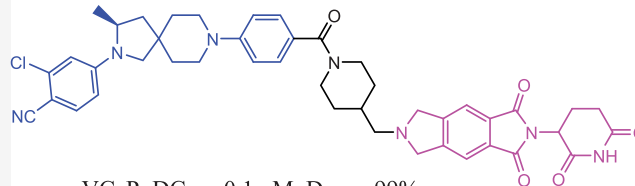
Article Recommendations



Supporting Information

**ABSTRACT:** We report herein the discovery and extensive characterization of ARD-1676, a highly potent and orally efficacious PROTAC degrader of the androgen receptor (AR). ARD-1676 was designed using a new class of AR ligands and a novel cereblon ligand. It has  $DC_{50}$  values of 0.1 and 1.1 nM in AR+ VCaP and LNCaP cell lines, respectively, and  $IC_{50}$  values of 11.5 and 2.8 nM in VCaP and LNCaP cell lines, respectively. ARD-1676 effectively induces degradation of a broad panel of clinically relevant AR mutants. ARD-1676 has an oral bioavailability of 67, 44, 31, and 99% in mice, rats, dogs, and monkeys, respectively. Oral administration of ARD-1676 effectively reduces the level of AR protein in the VCaP tumor tissue in mice and inhibits tumor growth in the VCaP mouse xenograft tumor model without any sign of toxicity. ARD-1676 is a highly promising development candidate for the treatment of AR+ human prostate cancer.

ARD-1676 (A Highly Potent and Orally Efficacious AR Degradator)



VCaP:  $DC_{50}$  = 0.1 nM,  $D_{max}$  = 99%.

LNCaP:  $DC_{50}$  = 1.1 nM,  $D_{max}$  = 98%

F value (%): 67 (mouse), 44 (rat), 31 (dog), 99 (monkey)

## INTRODUCTION

The androgen receptor (AR) and AR signaling play a pivotal role in the initiation and progression of human prostate cancer.<sup>1,2</sup> AR-targeted therapeutic agents, including abiraterone, which blocks androgen synthesis, and second-generation AR antagonists, such as enzalutamide, apalutamide, and darolutamide, have been developed for the treatment of advanced human prostate cancer.<sup>3</sup> While these agents have proved to be effective in the clinic, resistance to these drugs typically develops within 18 months.<sup>4</sup> Some of the major resistance mechanisms include AR gene amplification, AR-activating mutations, and expression of AR variants.<sup>5</sup> In the majority of human prostate cancers developed resistant to AR-targeted agents, AR and AR signaling continue to play a role in tumor progression, and novel therapeutic strategies to target AR and AR signaling are being sought.<sup>6</sup>

One attractive and novel strategy to target the AR is through induction of targeted protein degradation. Inspired by the clinical success of selective estrogen receptor degraders (SERDs) for the treatment of human breast cancers, selective AR degraders (SARDs) have been pursued. However, currently, SARD molecules still have relatively weak degradation potency and significant improvement is needed.<sup>7</sup>

A second approach to induce AR protein degradation is the use of the proteolysis-targeting chimera (PROTAC) technology. PROTAC agents are heterobifunctional molecules containing a ligand that binds to a protein of interest, a ligand that binds to and recruits an E3 ligase or an E3 ligase complex, and a linker that joins them together.<sup>8</sup> The first AR PROTAC molecule (**1**) was designed using a bicalutamide derivative as the AR ligand and an MDM2 inhibitor as the E3 ligase ligand (Figure 1).<sup>9,10</sup> While effective AR degradation of compound **1** was only achieved at micromolar concentrations,<sup>9</sup> it provided the important proof of concept that AR protein can be successfully degraded using the PROTAC technology.

Another AR degrader, named SNIPPER (**2**), was designed using a ligand to recruit a cellular inhibitor of apoptosis protein 1 (cIAP1) as the E3 ligase.<sup>11</sup> A limitation for an IAP-based AR degrader is that the cIAP1 protein itself can also be degraded by the IAP ligand used in the degrader molecule, thus limiting the

Received: July 12, 2023

Published: September 8, 2023



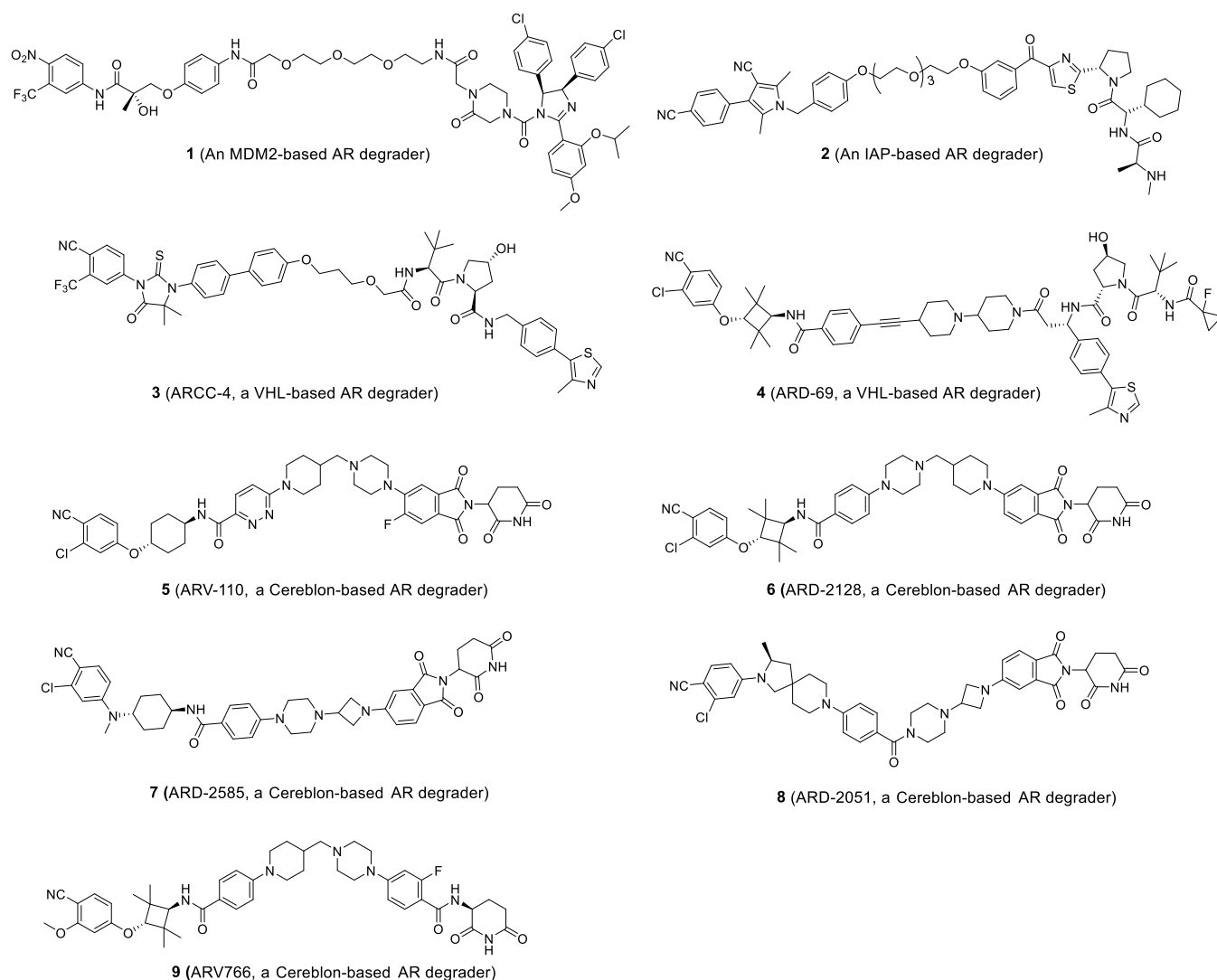


**Figure 1.** Representative AR PROTAC degraders.

degradation potency and efficacy against AR. Highly potent AR degraders have been reported using VHL ligands, which recruit the VHL/cullin 2 as the E3 ligase system, and such degrader molecules include ARCC-4 (3),<sup>6</sup> ARD-69 (4),<sup>12</sup> and ARD-266.<sup>13</sup> A significant limitation for VHL-based AR degraders is their poor oral bioavailability, which prevents their clinical development as oral agents. Potent PROTAC AR degraders have been discovered using cereblon ligands. In contrast to VHL-based PROTAC AR degraders, a number of reported PROTAC AR degraders, including ARV-110 (bavdegalutamide, 5),<sup>14,15</sup> ARD-2128 (6),<sup>16</sup> ARD-2585 (7),<sup>17</sup> and ARD-2051 (8),<sup>18</sup> have been found to achieve good oral bioavailability and upon oral administration effectively inhibit tumor growth in AR + human prostate cancer models in mice. Importantly, ARV-110 has been shown to be safe in phase 1/2 human clinical trials and has demonstrated clinical activity as a single agent in patients with tumors carrying AR double mutations. ARV-766 (9) is another orally bioavailable AR PROTAC from Arvinas that is being evaluated in phase 2 clinical trials, and its chemical structure was disclosed during the 2023 AACR conference.<sup>19,20</sup> A number of additional orally bioavailable PROTAC AR degraders, including CC94676,<sup>21–24</sup> HP518,<sup>25–27</sup> and AC0176<sup>28–31</sup> have progressed into human clinical trials.

Although their precise chemical structures have not been disclosed, published patents suggest that these compounds are likely cereblon-based degraders.

In this study, we report the design, synthesis, and evaluation of potent and orally bioavailable PROTAC AR degraders using a new class of AR ligands and novel cereblon ligands. Our efforts have led to the discovery of ARD-1676 as a highly potent and orally efficacious AR degrader. ARD-1676 demonstrates excellent oral bioavailability in mice, rats, dogs, and monkeys. ARD-1676 is effective in reducing the AR protein in tumor tissue and achieves strong antitumor activity in the AR+ VCaP xenograft model in mice with oral administration. ARD-1676 is a promising development candidate for the treatment of AR+ human prostate cancers and other AR-dependent human diseases or conditions.

## RESULTS AND DISCUSSION

**Design of a New Class of AR Ligands.** We previously reported our discovery of ARD-2585, a potent and orally efficacious PROTAC AR degrader.<sup>17</sup> In our further evaluations of ARD-2585 as a potential development candidate, we found that while it achieves excellent oral bioavailability in mice, it has only a modest oral bioavailability of 13% in rats, highlighting the

challenge underlying the development of orally bioavailable PROTAC AR degraders across different species.

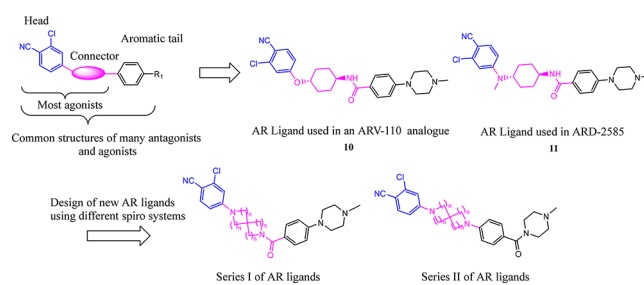
A typical cereblon-based PROTAC AR degrader consists of an AR ligand, a cereblon ligand, and a linker. In our previous studies, we performed extensive optimization of the linker which led to the discovery of ARD-2128<sup>16</sup> and ARD-2585.<sup>17</sup> In the present study, we aimed at designing novel AR ligands and new cereblon ligands with the objective of identifying PROTAC AR degraders, which not only achieve high AR degradation potency but also good oral bioavailability across species. Our goal was identification of one or more candidates suitable for clinical development.

Our recent comprehensive review<sup>32</sup> of previously reported AR agonists and antagonists showed that many AR ligands have some common structural features, namely, a substituted phenyl ring as the “head group”, an optional aromatic tail, and a connector (Table 1). A large number of AR agonists and antagonists, including a number of clinical compounds, contain a 4-cyano-3-chlorophenyl moiety as the head group. Although no co-crystal structure of antagonists with human AR has been reported, a number of co-crystal structures of AR agonists in a complex with the human AR are available.<sup>33</sup> These co-crystal structures show that the 4-cyano-3-chlorophenyl moiety in an agonist binds deeply into the AR ligand pocket and enjoys hydrogen bonding and hydrophobic interactions with the AR. In addition, our modeling suggested that the aromatic group in the tail portion of the AR ligand in ARD-2585 has  $\pi$ - $\pi$  interactions with Trp741 of the AR.<sup>17</sup> The connector between the head and tail groups in AR ligands is structurally diverse. Our modeling showed that the connector in the AR ligand used in ARD-2585 is in contact with a number of hydrophobic residues but has no specific hydrogen bonding interactions with the AR.<sup>17</sup>

We posited that AR ligands with a reduced polar surface and conformational flexibility may lead to improved oral bioavailability across species in resulting PROTAC degraders. Accordingly, we designed two series of AR ligands using spiro amines with a carbonyl group inserted on either side of the tail phenyl ring to reduce both the polar surface and conformational flexibility without increasing non-sp<sup>3</sup> atoms when compared to the AR ligand used in ARD-2585. In addition, a methyl piperazine group was introduced into our designed AR ligands to create a convenient site as an exit vector for the synthesis of PROTAC degraders and at the same time improve solubility of the resulting AR ligands. We synthesized a total of 13 new AR ligands and evaluated their binding affinities to the AR, obtaining the data summarized in Table 1.

Among those AR ligands in series I, compounds designed using 4,4-spiro (12 and 13), 4,6-spiro (15), 5,4-spiro (16), 6,4-spiro (19), and 6,6-spiro (21) as the connectors have no appreciable binding affinities to AR up to 10  $\mu$ M and thus have IC<sub>50</sub> > 10  $\mu$ M. Compounds designed using 4,5-spiro (14), 5,5-spiro (17), 5,6-spiro (18), and 6,5-spiro (20) connectors have IC<sub>50</sub> values of 9.9, 6.9, 3.6, and 5.0  $\mu$ M, respectively, and are therefore weak AR ligands. Among those AR ligands in series II, compounds containing a 5,5-spiro ring system (22) and 6,5-spiro ring system (24) have IC<sub>50</sub> values of 1.8 and 5.4  $\mu$ M, respectively, and are also weak AR ligands. However, compound 23 with a 5,6-spiro ring system was found to have an IC<sub>50</sub> value of 80 nM. In the same binding assay, AR ligands used in ARV-110 and ARD-2585 have IC<sub>50</sub> values of 55 and 15 nM, respectively, enzalutamide has an IC<sub>50</sub> value of 800 nM, and a potent AR agonist R1881<sup>34</sup> has an IC<sub>50</sub> of 5.0 nM. Hence, compound 23 is slightly weaker than AR ligands in ARV110 and

**Table 1. Novel AR Ligands with Different Spiro Ring Systems as Connectors and Their Binding Affinities to the AR<sup>a</sup>**



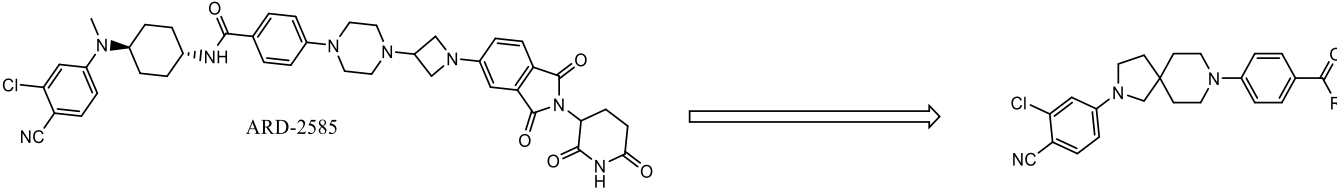
No	Code Name	Connector Structure	Series	AR-LBD binding IC <sub>50</sub> ( $\mu$ M)
10				0.055 $\pm$ 0.003
11				0.015 $\pm$ 0.002
12	AR4001		I	>10
13	AR4002		I	>10
14	AR4022		I	9.9 $\pm$ 4.9
15	AR4023		I	>10
16	AR4004		I	>10
17	AR4010		I	6.9 $\pm$ 3.6
18	AR4012		I	3.6 $\pm$ 0.7
19	AR4008		I	>10
20	AR4017		I	5.0 $\pm$ 2.1
21	AR4018		I	>10
22	AR4122		II	1.8 $\pm$ 1.0
23	AR4034		II	0.08 $\pm$ 0.01
24	AR4049		II	5.4 $\pm$ 0.8
	Enzalutamide			0.8
	R1881			0.005 $\pm$ 0.001

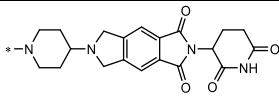
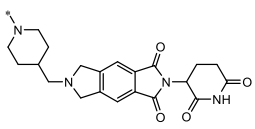
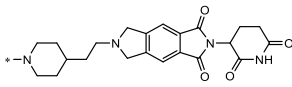
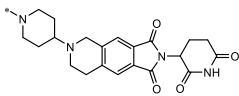
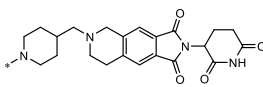
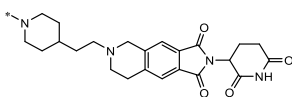
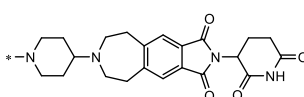
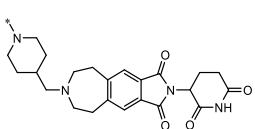
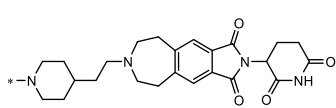
<sup>a</sup>All the data are an average of three independent experiments.

ARD-2585 but 10 times more potent than enzalutamide and thus a potent AR ligand. We modeled compound 23 in complex with the human AR.<sup>33</sup> Our predicted binding model suggested that the cyanophenyl ring and connector portion in compound 23 binds to the AR in a manner very similar to an AR ligand S1,



Table 3. Initial Series of AR PROTACs and Their Degradation in the VCaP Cell Line



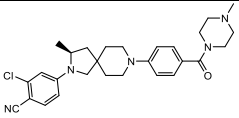
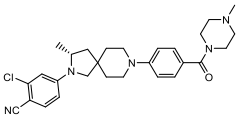
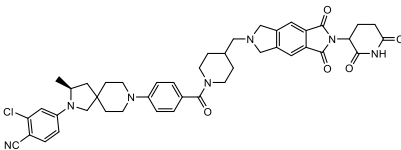
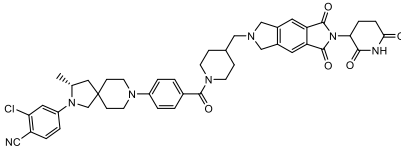
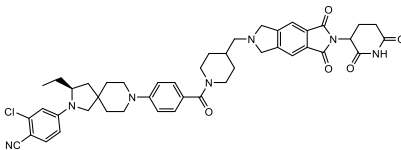
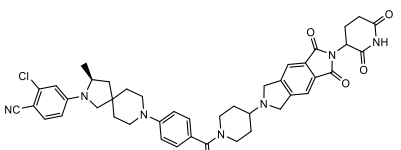
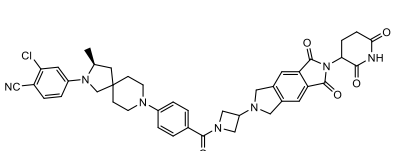
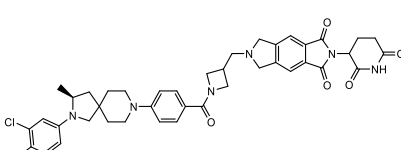
No	Compound	R	VCaP cell line (24 h)	
			DC <sub>50</sub> (nM)	D <sub>max</sub> (%)
30	ARD-1631		9.7	89
31	ARD-1632		5.7	88
32	ARD-1633		92	78
33	ARD-1628		73	63
34	ARD-1629		25	53
35	ARD-1630		125	79
36	ARD-4050		18	81
37	ARD-4051		51	51
38	ARD-4052		3 (μM)	76

In an attempt to further increase the degradation potency for AR degrader **31**, we modeled the AR ligand **23** in a complex with the AR. Our modeling suggested that the 5,6-spiro ring system in compound **23** binds to a hydrophobic environment, and there is also space available around the 5-membered ring for a small substituent (Figure S1). Accordingly, we synthesized *S*-**23a** with an *S*-methyl substitution and as its stereoisomer *R*-**23a**. In our AR binding assay, compound *S*-**23a** has IC<sub>50</sub> = 6.9 nM to the AR, whereas compound *R*-**23a** has IC<sub>50</sub> > 10 μM. Our modeling suggested that compound *S*-**23a** adopts a very similar pose as

compound **23** but captures additional hydrophobic interactions with the AR through its additional methyl group (Figure S4).

We next synthesized their corresponding degraders **39** and **40** by installation of either an *S*-methyl or an *R*-methyl substituent on the 5-membered ring in degrader **31**. Consistent with the high binding affinity of compound *S*-**23a** to the AR, the corresponding degrader **39** synthesized using the AR ligand *S*-**23a** has DC<sub>50</sub> = 0.1 nM and D<sub>max</sub> = 99% in the VCaP cell line and is therefore 57 times more potent than degrader **31** (Table 4 and Figure S5). In comparison, the corresponding degrader **40** synthesized using the AR ligand *R*-**23a** has DC<sub>50</sub> = 385 nM and

Table 4. Optimization of Degradar ARD-1632

No	Compound	Structure	VCaP cell line	
			DC <sub>50</sub> (nM)	D <sub>max</sub> (%)
	<b>S-23a</b>		NA	NA
	<b>R-23a</b>		NA	NA
<b>39</b>	ARD-1676		0.1	99
<b>40</b>	ARD-1719		385	81
<b>41</b>	ARD-1693		0.2	99
<b>42</b>	ARD-1671		0.4	91
<b>43</b>	ARD-1689		0.7	89
<b>44</b>	ARD-1690		0.5	99

$D_{\max} = 81\%$  and is therefore >3000 times less potent than degrader **39**.

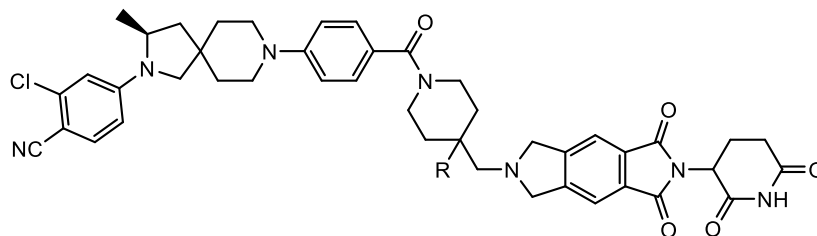
Encouraged by the exceptional degradation potency of degrader **39**, we replaced the *S*-methyl group in **39** with an *S*-ethyl substituent, yielding degrader **41**, which attained  $DC_{50} = 0.2$  nM and  $D_{\max} = 99\%$ . Hence, compound **41** is a highly potent and effective AR degrader but is slightly less potent than degrader **39**.

We next modified the linker in degrader **39**. Removal of one methylene group from the linker in degrader **39** yielded compound **42**, which has  $DC_{50} = 0.4$  nM and  $D_{\max} = 91\%$ .

Changing the 6-membered ring to a 4-membered ring in the linker in degraders **39** and **42** resulted in degraders **43** and **44**, which have  $DC_{50} = 0.7$  and  $0.5$  nM and  $D_{\max} = 89$  and  $99\%$ , respectively.

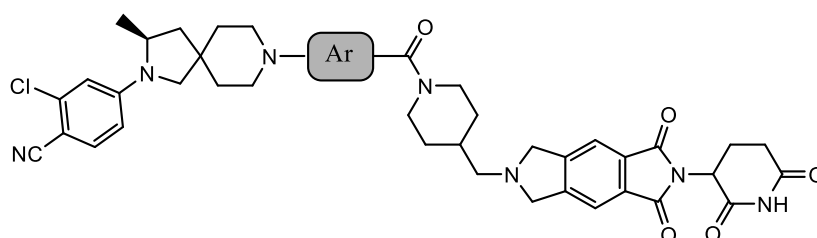
We performed further modifications of the linker in degrader **39** by introducing substituents on the linker piperidine ring (Table 5 and Figure S6). Substituents with fluorine, methoxy, and methyl on the linker resulted in compounds **45**, **46**, and **47**, respectively, which have  $DC_{50} = 0.9$ ,  $0.3$ , and  $3.8$  nM, respectively, and  $D_{\max} = 97$ – $99\%$ . However, degrader **48** with

Table 5. Further Optimization of the Linker in ARD-1676



no	compound	structures (R)	VCaP cell line	
			DC <sub>50</sub> (nM)	D <sub>max</sub> (%)
39	ARD-1676	H	0.1	99
45	ARD-1683	F	0.9	99
46	ARD-1684	OMe	0.3	99
47	ARD-1694	Me	3.8	97
48	ARD-1705	OH	290	71

Table 6. Introduction of Heteroatoms into the Central Phenyl Ring (AR) of ARD-1676



No	Compound	Structures (Ar)	VCaP cell line	
			DC <sub>50</sub> (nM)	D <sub>max</sub> (%)
39	ARD-1676		0.1	99
49	ARD-7063		2.7	99
50	ARD-7064		4.6	99
51	ARD-4055		15.6	99
52	ARD-4056		2.3	99

a hydroxy substituent has DC<sub>50</sub> = 290 nM and D<sub>max</sub> = 71% and is a much weaker degrader than other compounds in this series.

Next, we introduced heteroatoms into the central phenyl ring of **39** (Table 6 and Figure S7). Degradator **49** containing pyridazine, degrader **50** containing pyrimidine, and degraders **51** and **52** containing pyridine have DC<sub>50</sub> of 2.7, 4.6, 15.6, and 2.3 nM, respectively, and D<sub>max</sub> = 99%. Hence, while these compounds are clearly less potent than degrader **39**, they are still potent and effective AR degraders.

**Further Evaluation of Degradator 39 and Other Potent Degradators.** We next evaluated a number of potent AR degraders in the LNCaP AR+ prostate cancer cell line, which carries a T878A AR mutation, and obtained the data summarized in Table 7 and Figure S8. Degradators **39**, **41**–**47**, and **49**–**52** have DC<sub>50</sub> values = 0.5–8.9 nM and D<sub>max</sub> = 93–99%

Table 7. AR Degradation Activity of Representative, Potent Degradators in the LNCaP Cell Line

no	compound	degradation in LNCaP		no	compound	degradation in LNCaP	
		DC <sub>50</sub> (nM)	D <sub>max</sub> (%)			DC <sub>50</sub> (nM)	D <sub>max</sub> (%)
39	ARD-1676	1.1	98	46	ARD-1684	1.0	97
41	ARD-1693	3.5	99	47	ARD-1694	8.9	94
42	ARD-1671	0.8	97	49	ARD-7063	0.5	99
43	ARD-1689	5.0	93	50	ARD-7064	1.2	99
44	ARD-1690	2.9	99	51	ARD-4055	4.6	99
45	ARD-1683	3.7	96	52	ARD-4056	2.2	99
5	ARV-110	1.5	99				

in the LNCaP cell line. Among them, degraders **39**, **42**, **46**, **49**, and **50** have  $DC_{50}$  values of 0.5–1.2 nM and  $D_{max}$  values of >95% and are highly potent and effective AR degraders.

We evaluated these 12 most potent degraders for their cell growth inhibition in the VCaP cell line with ARV-110 included as the control and obtained the data summarized in Table 8. Degraders **39**, **41–47**, and **49–52** have  $IC_{50} = 4.9–85$  nM, whereas ARV-110 has an  $IC_{50}$  value of 16.2 nM.

**Table 8. Cell Growth Inhibitory Activity of Selected Degraders in the VCaP Cell Line<sup>a</sup>**

no.	compound	$IC_{50}$ (nM) in VCaP cells	no.	compound	$IC_{50}$ (nM) in VCaP cells
39	ARD-1676	11.5 ± 0.3	46	ARD-1684	4.9 ± 0.3
41	ARD-1693	23 ± 2	47	ARD-1694	42 ± 0.0
42	ARD-1671	16.5 ± 1.5	49	ARD-7063	20 ± 1
43	ARD-1689	85 ± 3	50	ARD-7064	10 ± 1
44	ARD-1690	25.7 ± 0.6	51	ARD-4055	46 ± 11
45	ARD-1683	18 ± 2	52	ARD-4056	11 ± 0.2
5	ARV-110	16.2 ± 1.5			

<sup>a</sup>All the data are an average of three independent experiments.

### Pharmacokinetic (PK) Studies of Potent AR Degraders

**in Rats.** As indicated above, while ARD-2585 has excellent oral exposure in mice,<sup>17</sup> it has only a moderate oral bioavailability of 13% in rats (Table 9). Therefore, to identify potent AR degraders with an excellent overall PK profile, we performed pharmacokinetic studies of 9 potent new PROTAC AR degraders (**39**, **42–47**, and **49–50**) identified from this study in rats, with ARV-110 included as a control compound. The obtained PK data are summarized in Table 9.

Among these 9 compounds, compounds **39**, **42**, and **47** show the best oral bioavailability and an excellent overall PK profile. Upon intravenous administration at 2 mg/kg, degrader **39** (ARD-1676) has a low clearance of 0.36 L/h/kg, a moderate  $V_{ss} = 1.7$  L/kg, and a reasonably long  $T_{1/2} = 4.5$  h. With a 5 mg/kg oral administration, **39** achieves a high  $C_{max} = 871$  ng/mL, an  $AUC > 6$   $\mu$ g/mL·h, and an oral bioavailability ( $F$ ) of 44%. Compared to compound **39**, degrader **42** (ARD-1671) has a higher clearance ( $Cl = 0.92$  L/h/kg) and a larger volume of distribution ( $V_{ss} = 6.1$  L/kg) with intravenous administration and a modestly lower  $C_{max}$  and  $AUC$  with oral administration and has an oral bioavailability of 81%. Compound **47** (ARD-

1694) has a similar IV and oral PK profile as compound **39** (ARD-1676) and achieves an oral bioavailability of 45%. Compounds **45**, **46**, and **49** have moderate oral bioavailability based on their  $C_{max}$  and  $AUC$  values and their  $F$  values of 18–36%. Three other degraders (**43**, **44**, and **50**) were found to have low oral bioavailability based on their  $C_{max}$  and  $AUC$  values and their  $F$  values (7–15%). In our PK study, ARV-110 has a longer  $T_{1/2}$  than degraders **39**, **42**, and **47** in both IV and oral routes of administration, an excellent  $V_{ss}$  of 4.6 L/kg, a low clearance of 0.36 L/h/kg, and a similar overall oral bioavailability as compared to that of degraders **39**, **42**, and **47**.

Among degraders **39** (ARD-1676), **42** (ARD-1671), and **47** (ARD-1694) which have an excellent PK profile in rats, compound **39** has the best degradation potency and cell growth inhibitory activity. We therefore decided to perform extensive evaluations of **39** (ARD-1676) as a potential development candidate.

### Further Evaluation of ARD-1676 in AR+ Prostate Cancer Cell Lines.

We evaluated the AR degradation and cell growth inhibition of ARD-1676 in the LNCaP cell line, which carries a T878A AR mutation, with ARV-110 included as the control. ARD-1676 attains  $DC_{50} = 1.1$  nM and  $D_{max} = 98\%$  in AR degradation and  $IC_{50} = 2.8$  nM in cell growth inhibition in the LNCaP cell line. In comparison, ARV-110 has  $DC_{50} = 1.5$  nM and  $D_{max} = 99\%$  in AR degradation and  $IC_{50} = 18.5$  nM in cell growth inhibition in the LNCaP cell line (Figures 2 and S9). In the same assay, enzalutamide has  $IC_{50} = 213$  nM in cell growth inhibition in the LNCaP cell line.

We further evaluated the activity of ARD-1676 in the MDA-Pca-2b cell line with AR double mutations (L702H and T878A) (Figures 3 and S9). ARD-1676 has  $DC_{50} = 8$  nM and  $D_{max} > 95\%$  in the MDA-Pca-2b cell line, indicating that ARD-1676 is effective in inducing degradation of the AR double mutant protein (L702H and T878A). In comparison, ARV-110 is ineffective in reducing the AR double mutant protein in the MDA-Pca-2b cell line (Figure S9).

We evaluated ARD-1676 for its degradation kinetics in the VCaP and LNCaP cell lines with the data shown in Figure 4. ARD-1676 effectively degraded >50% of the AR after a 1 h treatment time and achieved maximum degradation with a 3–6 h treatment time in both the VCaP and LNCaP cell lines at 10 and 100 nM (Figure 4). Hence, ARD-1676 induces rapid degradation of AR protein in both the VCaP and LNCaP cell lines.

**Table 9. Pharmacodynamic Parameters of Potent AR Degraders in Rats<sup>a</sup>**

male rats	IV (mg/kg)	$T_{1/2}$ (h)	$AUC_{(0-t)}$ (h·ng/mL)	$V_{ss}$ (L/kg)	Cl (L/h/kg)	PO (mg/kg)	$T_{1/2}$ (h)	$C_{max}$ (ng/mL)	$AUC_{(0-t)}$ (h·ng/mL)	$F$ %	
39	ARD-1676	2	4.5	5492	1.7	0.36	5	5.6	871	6016	44
42	ARD-1671	2	5.5	2105	6.1	0.92	5	5.5	410	4279	81
43	ARD-1689	2	3.2	2367	2.7	0.87	5	1.89	94	423	7.2
44	ARD-1690	2	1.4	1375	1.8	1.50	5	1.20	78	310	9.0
45	ARD-1683	2	7.9	4003	4.2	0.47	5	5.2	216	1822	18
46	ARD-1684	2	4.9	2388	4.1	0.83	5	5.6	179	1317	22
47	ARD-1694	2	6.1	5090	3.1	0.38	5	8.4	539	5731	45
49	ARD-7063	1	2.0	1010	2.2	1.94	3	1.4	247	1097	36
50	ARD-7064	1	1.4	495	2.3	2.00	3	1.2	55	235	15
5	ARV-110	1	12	2272	4.6	0.36	3	27.1	280	3595	52
7	ARD-2585	1	5.5	1302	5.3	0.75	3	6.9	57	535	13

<sup>a</sup>Vehicle: 10% PEG400 + 90% PBS (pH 8).  $C_{max}$ , maximum drug concentration;  $AUC_{0-24h}$ , area under the curve between 0 and 24 h; Cl = plasma clearance rate;  $V_{ss}$  = steady-state volume of distribution;  $T_{1/2}$  = terminal half-life;  $F$  = oral bioavailability; IV, intravenous administration; PO, oral administration.

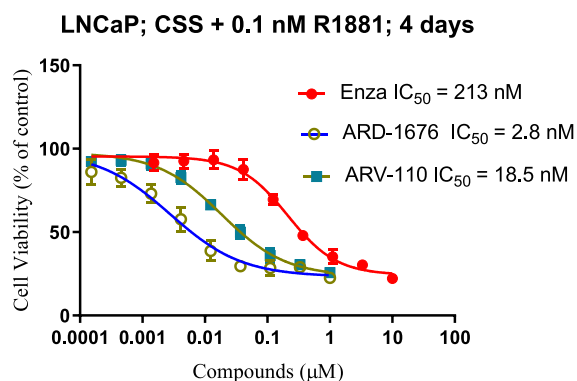


**Figure 2.** Cell growth inhibitory activities of ARD-1676 and controls ARV-110 and enzalutamide (Enza).

**Evaluation of ARD-1676 against a Broad Panel of AR Mutants in HEK293 Cells.** We next evaluated ARD-1676 for its ability to induce degradation against a broad panel of clinically relevant AR mutants in HEK293 cells. For this purpose, different AR mutants were overexpressed in HEK293 cells. The data are summarized in Figure 5.

Consistent with the data obtained in the VCaP cell line, ARD-1676 was highly effective in reducing the wild-type AR protein at concentrations as low as 1 nM in HEK293 cells with overexpressed AR protein. We constructed overexpression vectors for commonly observed AR mutations and deletions in the clinic in our in-house metastatic prostate cancer patient samples.<sup>35</sup> Two N-terminal mutations, K388R and the 388–390 deletion ( $\Delta$ 388–390), both disrupt a known AR-sumoylation site and are known to increase AR activity.<sup>36</sup> A number of common ligand-binding domain mutations allow for promiscuous ligand binding, allowing for resistance to standard AR antagonists: L702H (glucocorticoid-activated), V716M (conferring resistance to flutamide and bicalutamide), W742C (conferring resistance to bicalutamide), H875Y (activated by DHEA, estradiol, progesterone, flutamide, and nilutamide and found in CWR-R1 and CWR-22Rv1 cell lines), F877L (activated by enzalutamide), T878A (activated by DHEA, estradiol, progesterone, cyproterone acetate, flutamide, nilutamide, cholesterol, and other hydrophobic molecules), S889G (conferring bicalutamide resistance), and one large deletion of the ligand-binding domain that prevents broad antagonist binding,  $\Delta$ 873–879.<sup>35,37–39</sup> ARD-1676 was found to be highly effective and potent in reducing the K388R-, V716M-, W742C-, H875Y-, F877L-, and T878A-mutated AR proteins at concentrations as low as 1 nM. ARD-1676 effectively depleted two AR mutants with  $\Delta$ 388–390 and  $\Delta$ 873–879 deletion, respectively. While ARD-1676 was still capable of reducing the levels of AR L702H- and S889G-mutated AR proteins, it was much less effective as compared to its ability to reduce other AR-mutated proteins examined.

Taken together, using engineered cell lines, our data showed that ARD-1676 is highly effective and potent in depletion of the majority of AR-mutated proteins examined, suggesting its broad therapeutic potential in overcoming resistance conferred by these AR mutations to current AR-targeted agents.

**Confirmation of the PROTAC Mechanism of Action for ARD-1676.** We investigated the mechanism of AR degradation induced by ARD-1676. Our data (Figure 6) showed that AR degradation induced by ARD-1676 is effectively blocked by enzalutamide (an AR antagonist), thalidomide (a cereblon ligand), MG132 (a proteasome inhibitor), and MLN4924 (a NEDD8 inhibitor) in the VCaP cell line. These data demonstrated that ARD-1676 is a bona fide PROTAC AR degrader.

**RT-qPCR Analysis of AR-Regulated Genes by ARD-1676.** By depletion of AR protein in AR+ cells, AR degraders are expected to effectively suppress AR-regulated genes. We investigated the ability of ARD-1676 to suppress AR-regulated gene expression in the VCaP and LNCaP cell lines with the AR antagonist enzalutamide included as the control. The obtained data are summarized in Figure 7.

Our data showed that ARD-1676 effectively suppresses the expression of *KLK3*, which encodes PSA and *TMPRSS2* genes in both the VCaP and LNCaP cell lines in a concentration-dependent manner. ARD-1676 reduces the mRNA level of both *KLK3* and *TMPRSS2* genes by >50% at 1 nM in the VCaP cell line and 3 nM in the LNCaP cell line, respectively. In comparison, ARD-1676 is ~100-fold more potent than enzalutamide in suppressing the expression of these AR-regulated genes.

**Proteomic Analysis of Degradation Selectivity of the AR in the VCaP Cell Line.** We investigated the degradation selectivity of ARD-1676 by an unbiased proteomics analysis in the VCaP cell line with its corresponding inhibitor S-23a included as the control. The results are summarized in Figure 8.

With either 100 nM or 1  $\mu$ M ARD-1676, AR protein was reduced by >75%. Interestingly, PCLAF (PCNA clamp-associated factor, also known as PAF15/KIAA0101) and PLOD2 (procollagen-lysine 2-oxoglutarate 5-dioxygenase 2) were reduced by  $\geq$ 60% with 100 nM ARD-1676. However, these two proteins were not reduced significantly with 1  $\mu$ M ARD-1676. In addition to AR protein, the HAUS8 (augmin-like complex subunit 8) protein was reduced by 59% upon treatment with 1  $\mu$ M ARD-1676 but not by treatment with 100 nM ARD-1676. The significance of reduction of these three proteins by ARD-1676 requires further investigation. In comparison, AR ligand S-23a at 10  $\mu$ M failed to significantly reduce the levels of any of the proteins. Taken together, our global proteomic analysis showed that ARD-1676 is a selective AR degrader among the >5500 proteins that were analyzed.

**Evaluation of ARD-1676 for Its ADME Properties and hERG Inhibition.** We evaluated ARD-1676 for its ADME properties with obtained data summarized in Table 10.

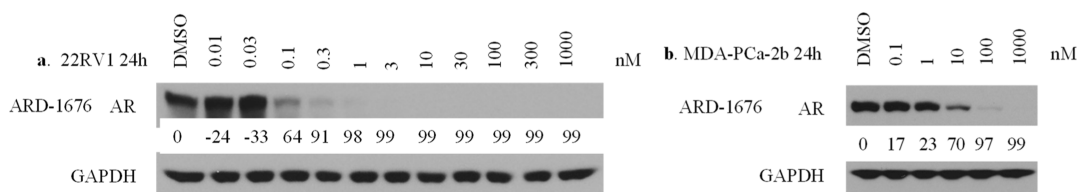


**Figure 3.** Western blotting of ARD-1676 degradation in (a) 22RV1 and (b) MDA-Pca-2b cell lines.

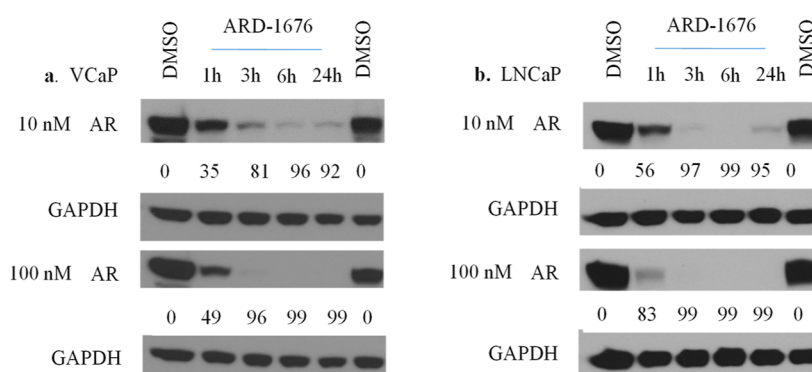


**Figure 4.** Degradation kinetics of ARD-1676 in (a) VCaP and (b) LNCaP cell lines.

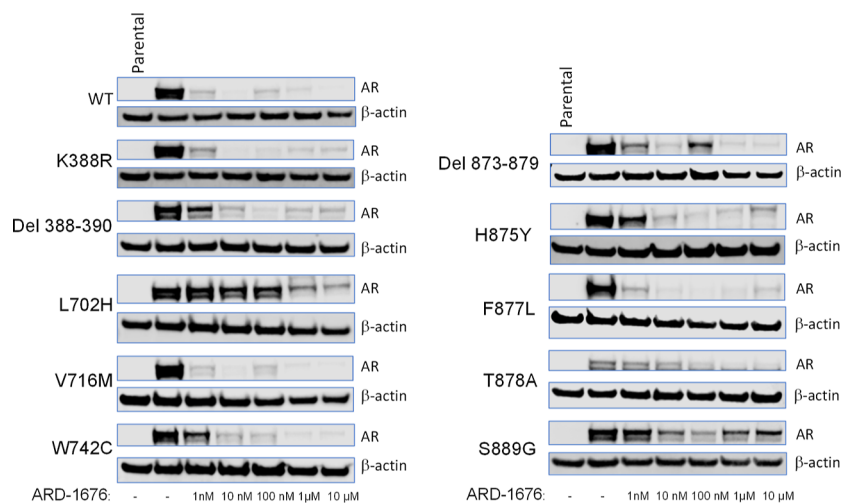


**Figure 5.** Effect of ARD-1676 on different AR mutant proteins in HEK293 cell lines overexpressed with different AR mutants. HEK293 cells overexpressing AR and clinically relevant AR mutations via lentivirus (pLV[Exp]-Puro-CMV > {hAR[NM\_000044.3]}—with individual mutations or wild type, Vector Builder, Inc., Chicago, IL) treated with ARD-1676 for 24 h in the presence of 50  $\mu\text{g}/\text{mL}$  cyclohexamide prior to total protein lysis [after 1 ng/mL puromycin (Fisher Scientific) selection]. Western blots using AR-XP (Cell Signaling) and  $\beta$ -actin (Sigma-Aldrich) primary antibodies and imaged using a Licor system (Omaha, NE) and secondary antibodies.

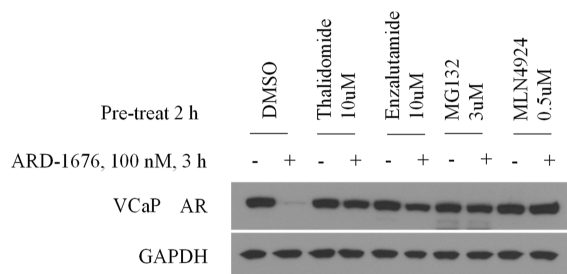


**Figure 6.** Evaluation of the mechanism of action of ARD-1676 in the VCaP cell line. VCaP cells were pretreated for 2 h with DMSO, an AR antagonist enzalutamide (10  $\mu\text{M}$ ), a cereblon ligand thalidomide (10  $\mu\text{M}$ ), a proteasome inhibitor MG-132 (3  $\mu\text{M}$ ), and an E1 neddylation inhibitor MLN4924 (0.5  $\mu\text{M}$ ). Cells were then treated for 3 h with ARD-1676 at 100 nM prior to western blotting analysis of AR protein with GAPDH used as the loading control.

Our data showed that while ARD-1676 has a low passive cell permeability, it has a low potential as a P-glycoprotein (Pgp) substrate.

We evaluated ARD-1676 for its liver microsomal, hepatocyte, and plasma stability in mouse, rat, dog, non-human primate (NHP), and human species. Our data showed that ARD-1676

has excellent microsomal, hepatocyte, and plasma stability in all these 5 species.

We evaluated ARD-1676 for its cytochrome P450 (CYP) inhibition against all the major CYP isoforms and found that ARD-1676 has no inhibition against any of the CYP isoforms evaluated.

Inhibition of the human *ether-à-go-go*-related gene human (hERG) by a drug molecule can lead to QT prolongation in the clinic, which is a major adverse event. We evaluated the inhibition of ARD-1676 for its potential hERG inhibition *in vitro*. Our data showed that ARD-1676 at both 3 and 30  $\mu\text{M}$  has negligible inhibition as compared to the control, indicating that ARD-1676 has no hERG liability.

Taken together, our data show that ARD-1676 has no ADME or hERG liability.

**Pharmacokinetic Evaluation of ARD-1676 in Mice, Dogs, and Monkeys.** In addition to the PK data for ARD-1676 in rats (Table 9), we further evaluated its pharmacokinetics (PK) in male ICR mice, male beagle dogs, and male cynomolgus monkeys and obtained the PK data summarized in Table 11.

In mice, ARD-1676 has a very low clearance ( $\text{Cl} = 0.04 \text{ L}/\text{h}/\text{kg}$ ), a modest volume of distribution ( $V_{\text{ss}} = 0.23 \text{ L}/\text{kg}$ ), a reasonably long  $T_{1/2}$  of 4.3–4.4 h with both IV and PO routes of administration, an excellent oral exposure with  $C_{\text{max}} = 9124 \text{ ng}/$

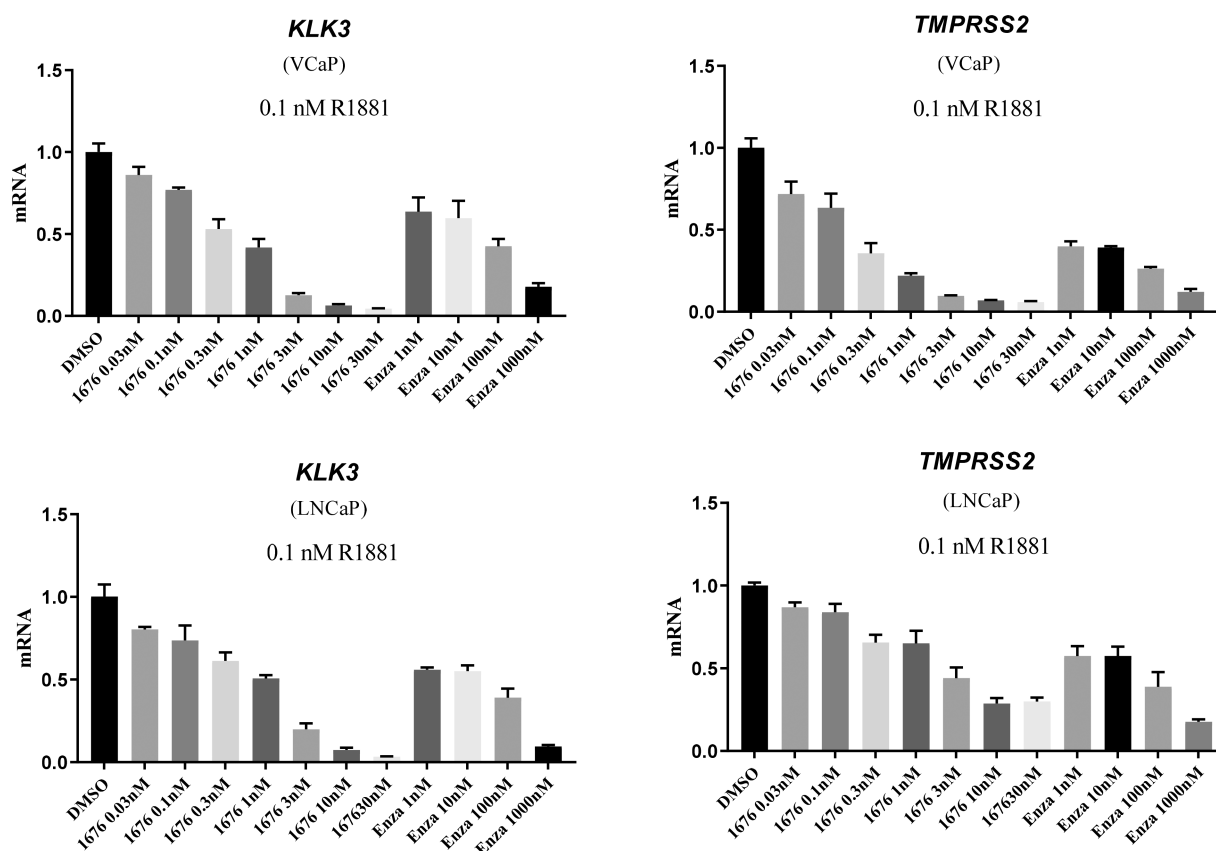


**Figure 7.** Suppression of *KLK3* (PSA) and *TMPRSS2* genes by ARD-1676 and enzalutamide in the AR+ VCaP and LNCaP cell lines. VCaP and LNCaP cells were treated in the presence of 0.1 nM R1881 for 24 h, and quantitative real-time polymerase chain reaction (qRT-PCR) was performed to determine the mRNA levels for *KLK3* and *TMPRSS2* genes.

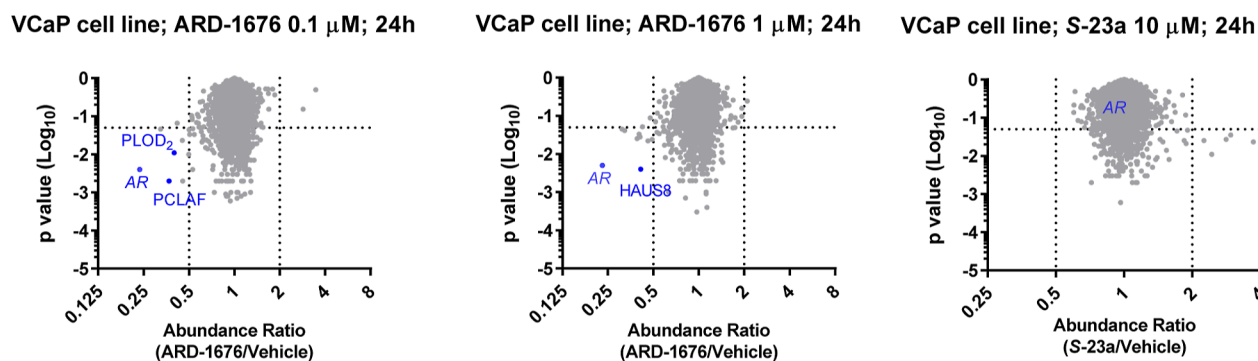


**Figure 8.** Proteomic analysis of ARD-1676 and its corresponding inhibitor (*S-23a*) in VCaP cells. VCaP cells were treated with ARD-1676 at 100 nM or 1  $\mu$ M or with *S-23a* at 10  $\mu$ M for proteomic analysis. Relative abundance of protein levels was normalized to DMSO-treated cells.

mL and AUC = 85 243 h·ng/mL dosed at 5 mg/kg, and an oral bioavailability of 67%.

In dogs, ARD-1676 has a low clearance ( $Cl = 0.19$  L/h/kg), a moderate volume of distribution ( $V_{ss} = 1.7$  L/kg), an extended  $T_{1/2}$  of 9.9 h with IV administration, a very long  $T_{1/2}$  of 27.4 h with PO administration, a good oral exposure with  $C_{max} = 1031$  ng/mL and AUC = 15 170 h·ng/mL dosed at 10 mg/kg, and an oral bioavailability of 31%.

In monkeys, ARD-1676 has a low clearance ( $Cl = 0.2$  L/h/kg), a moderate volume of distribution ( $V_{ss} = 2.1$  L/kg), a long  $T_{1/2}$  of 9.6–9.9 h with both IV and PO administration, an outstanding oral exposure with  $C_{max} = 1520$  ng/mL and AUC = 10 302 h·ng/mL dosed at 2 mg/kg, and an oral bioavailability of 99%.

**Pharmacodynamics and Antitumor Efficacy of ARD-1676 in Mice.** We next examined the pharmacodynamic (PD) effect of ARD-1676 in the VCaP xenograft tumor tissue in mice with the data summarized in Figure 9.

A single 12.5 mg/kg dose of ARD-1676 was orally administered in mice bearing the VCaP xenograft tumors. Western blotting analysis of the tumor tissues showed that ARD-1676 effectively reduces the AR protein level by 96 and 93% at 6 and 24 h time points, respectively.

Based on the PD data from ARD-1676, we determined its antitumor activity in the VCaP xenograft tumor model in mice and obtained the data summarized in Figure 10. The efficacy data showed that ARD-1676 effectively and dose-dependently inhibits tumor growth at all the 3 doses evaluated (Figure 10a).

Table 10. ADME and hERG Inhibitory Data for ARD-1676

permeability data in Caco-2 cells			hERG inhibitory activity data					
$P_{app}$ A-B ( $10^{-6}$ cm/s)	$P_{app}$ B-A ( $10^{-6}$ cm/s)	efflux ratio	ARD-1676 concentration		3 $\mu$ M	30 $\mu$ M		
0.07	0.13	1.8	hERG (% inhibition)		1	3		
stability in liver microsomes, hepatocytes, and plasma								
species		mouse	rat	dog	NHP	human		
liver microsome stability	$T_{1/2}$ (min)	>60	>60	>60	>60	>60		
	remain at 120 min (%)	82	87	87	82	84		
hepatocyte stability	$T_{1/2}$ (min)	>120	>120	>120	>120	>120		
plasma stability	$T_{1/2}$ (min)	>120	>120	>120	>120	>120		
	remain at 120 min (%)	62	52	71	92	69		
CYP inhibitory activity								
	CYP1A2	CYP2B6	CYP2C8	CYP2C9	CYP2C19	CYP2D6	CYP3A4 (midazolam)	CYP3A4 (testosterone)
IC <sub>50</sub> ( $\mu$ M)	>10	>10	>10	>10	>10	>10	>10	>10

Table 11. Pharmacokinetics Parameters of ARD-1676 in Mice, Rats, Dogs, and Monkeys

ARD-1676	IV (mg/kg) <sup>a</sup>	$T_{1/2}$ (h)	AUC <sub>(0-t)</sub> (h·ng/mL)	$V_{ss}$ (L/kg)	Cl (L/h/kg)	PO (mg/kg)	$T_{max}$ (h)	$T_{1/2}$ (h)	$C_{max}$ (ng/mL)	AUC <sub>(0-t)</sub> (h·ng/mL)	F %
ICR mice	2	4.3	50 538	0.23	0.04	5 <sup>a</sup>	2.0	4.4	9124	85 243	67
SD rat	2	4.5	5492	1.7	0.36	5 <sup>a</sup>	4.0	5.6	871	6016	44
beagle dog	1	9.9	4857	1.74	0.19	10 <sup>b</sup>	3.0	27.4	1031	15 170	31
NHP	1	10	5171	2.07	0.2	2 <sup>c</sup>	3.33	9.62	1520	10 302	99

<sup>a</sup>Vehicle: 10% PEG400 + 90% PBS (pH 8). <sup>b</sup>Vehicle: 50% PEG400 + 50% (40% HP- $\beta$ -CD in water). <sup>c</sup>Vehicle: 75% gelucire + 25% propylene glycol.  $C_{max}$ , maximum drug concentration; AUC<sub>0-24h</sub>, area under the curve between 0 and 24 h; Cl = plasma clearance rate;  $V_{ss}$  = steady-state volume of distribution;  $T_{1/2}$  = terminal half-life; F = oral bioavailability; IV, intravenous administration; PO, oral administration. NHP: cynomolgus monkey.

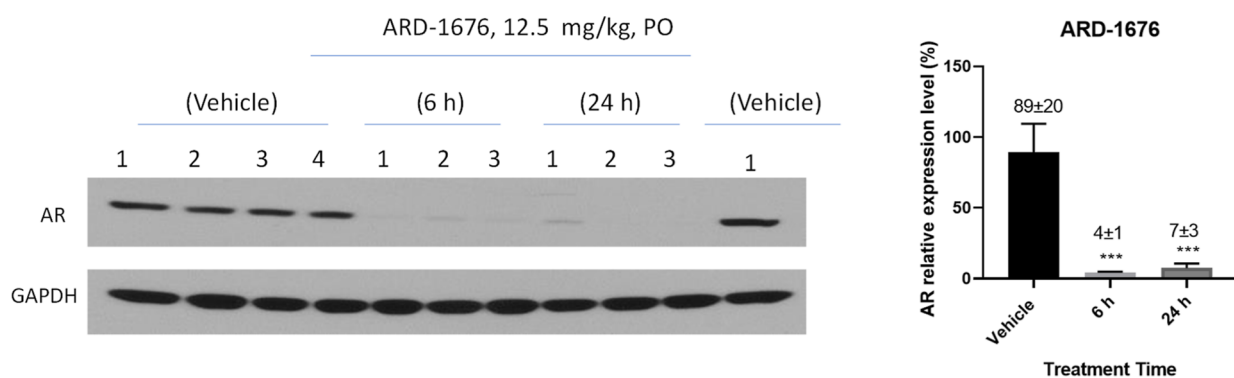


Figure 9. Pharmacodynamics of ARD-1676 in VCaP xenograft tumor tissues in mice. Tumor tissues were collected after 6 and 24 h upon oral administration of 12.5 mg/kg ARD-1676.

ARD-1676 suppressed tumor growth with a tumor growth inhibition (TGI) of 50, 68, and 85% at 10, 20, and 40 mg/kg, respectively, at the end of the treatment. ARD-1676 is well tolerated in this efficacy experiment and does not cause animal weight loss or other signs of toxicity during the entire experiment (Figure 10b). In comparison, ARV-110 suppresses VCaP xenograft tumor growth with a TGI of 47% at 10 mg/kg (Figure S10).

## CHEMISTRY

The synthesis of AR ligands 12–24 is shown in Scheme 1. Nucleophilic substitution of the fluorine in 53 with amines in spiro 54 followed by deprotection of Boc affords the free amine (55). HATU-assisted amide coupling of the amine in 55 with 4-(4-methylpiperazin-1-yl)benzoic acid provides AR ligands 12–21. Buchwald coupling of the amine in 55 with *tert*-butyl 4-iodobenzoate followed by TFA-assisted deprotection of the *t*-

butyl ester affords 56 and amide coupling of the acids (56) with 1-methylpiperazine provides the AR ligands (22–24).

Dipropargyl amine (59) cyclizes with dimethyl acetylenedicarboxylate under Wilkinson's catalyst (RhCl(PPh<sub>3</sub>)<sub>3</sub>) to form an isoindoline dicarboxylate (61) (Scheme 2).<sup>40,41</sup> Dipropargyl amine (59) in turn is synthesized by nucleophilic substitution of propargyl amine (57) by propargyl bromide (58). The dicarboxylate (61) cyclizes with the amine in 62 to form 63 after deprotection of the Boc group. Methylation of the amine in 63 affords the cereblon ligand (27).

Cyclization of the bromoaldehyde (64) with 65 affords the isoquinoline (66), which undergoes PtO<sub>2</sub>-catalyzed hydrogenation to provide 67 (Scheme 3).<sup>42</sup> The dicarboxylate (67) cyclizes with the amine in 62 to form 68 after deprotection of the Boc group. Methylation of the amine in 68 affords the cereblon ligand (28).

Double Suzuki coupling of 69 with 70 affords 71 (Scheme 4).<sup>43</sup> Deprotection by hydrogenation of the benzyl group,

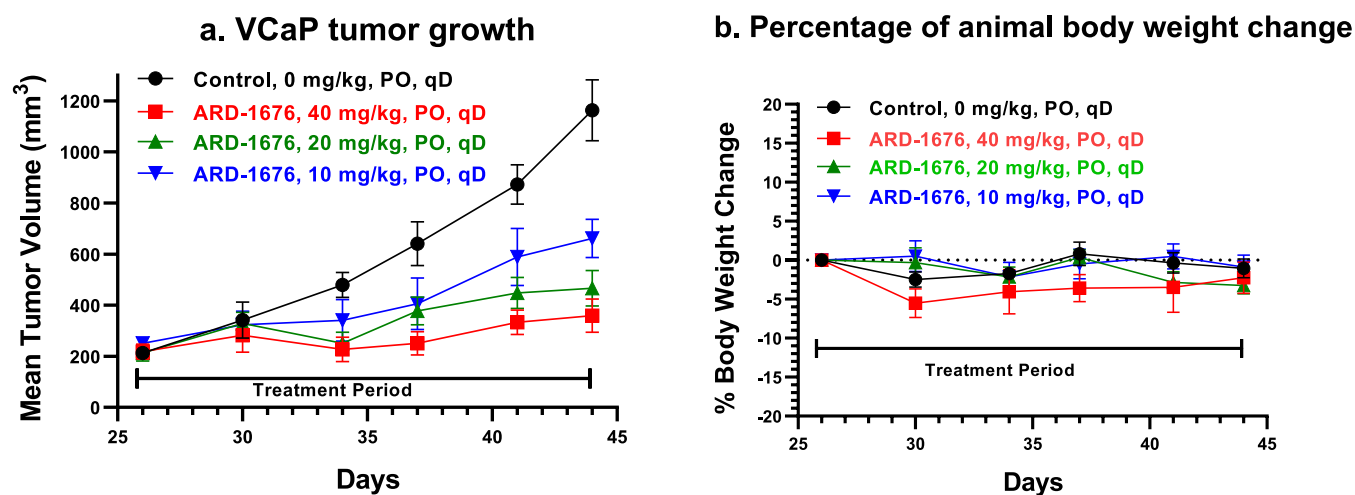
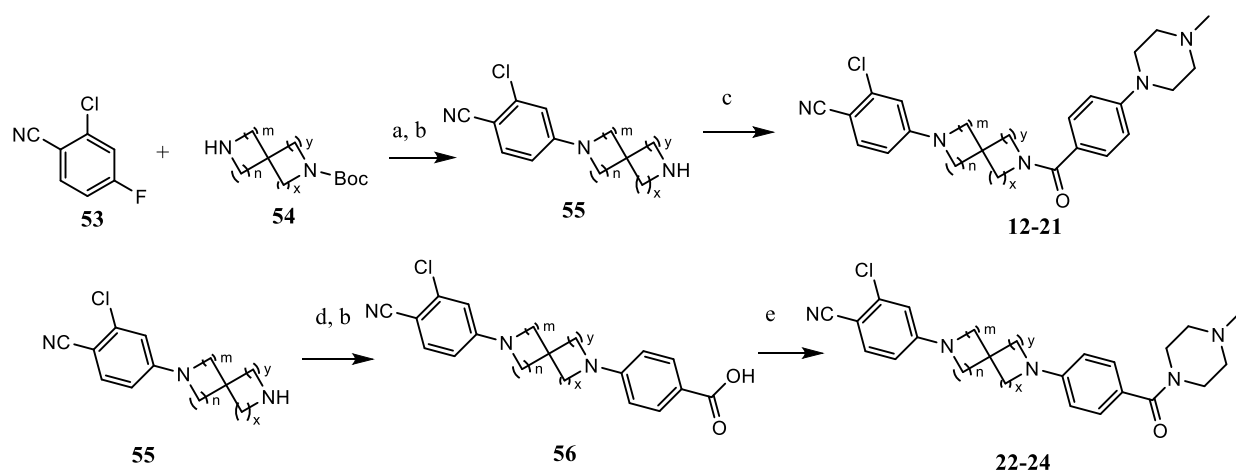


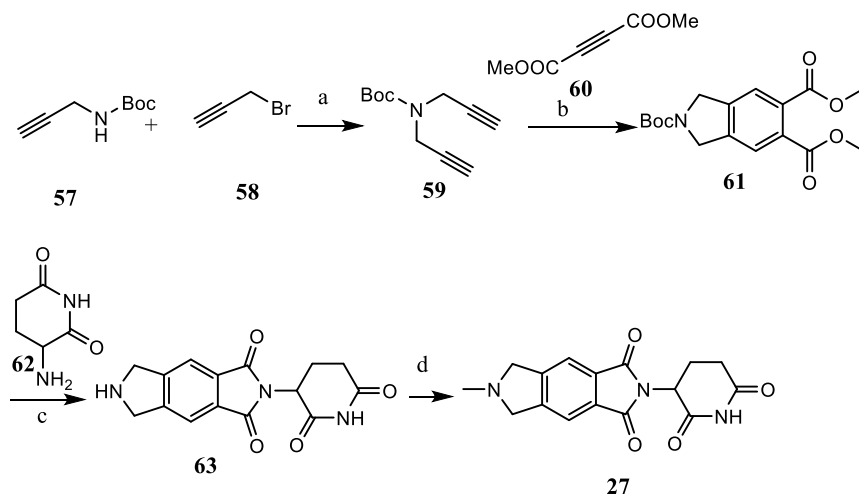
Figure 10. Antitumor activity of ARD-1676 in the VCaP xenograft tumor model in SCID mice. ARD-1676 was administered via oral gavage daily for a total of 21 days. (a) Tumor growth. (b) Percentage of animal body weight change.

### Scheme 1. Synthesis of AR Ligands 12–24<sup>a</sup>

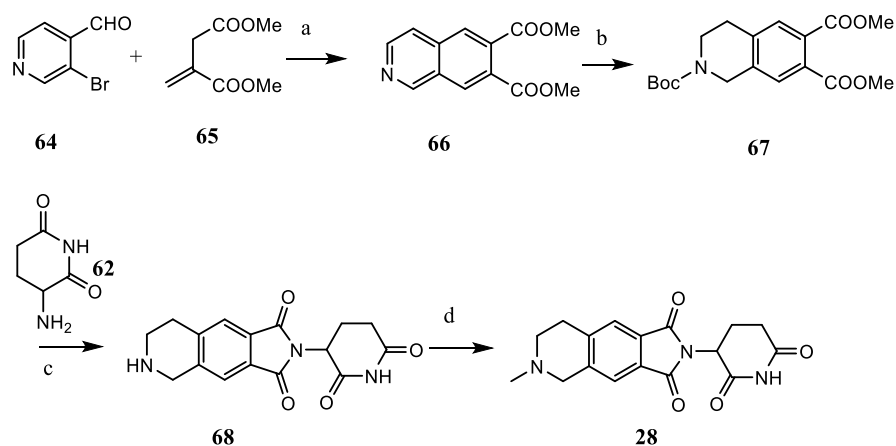


<sup>a</sup>Reaction conditions: (a) DMF, Cs<sub>2</sub>CO<sub>3</sub>, 110 °C, 16 h; (b) DCM, TFA; (c) DCM, 4-(4-methylpiperazin-1-yl)benzoic acid, HATU, DIPEA, rt, 0.5 h; (d) dioxane, *tert*-butyl 4-iodobenzoate, Pd<sub>2</sub>(dba)<sub>3</sub>, Xphos, Cs<sub>2</sub>CO<sub>3</sub>, 100 °C, 12 h; (e) DCM, 1-methylpiperazine, HATU, DIPEA, rt, 0.5 h.

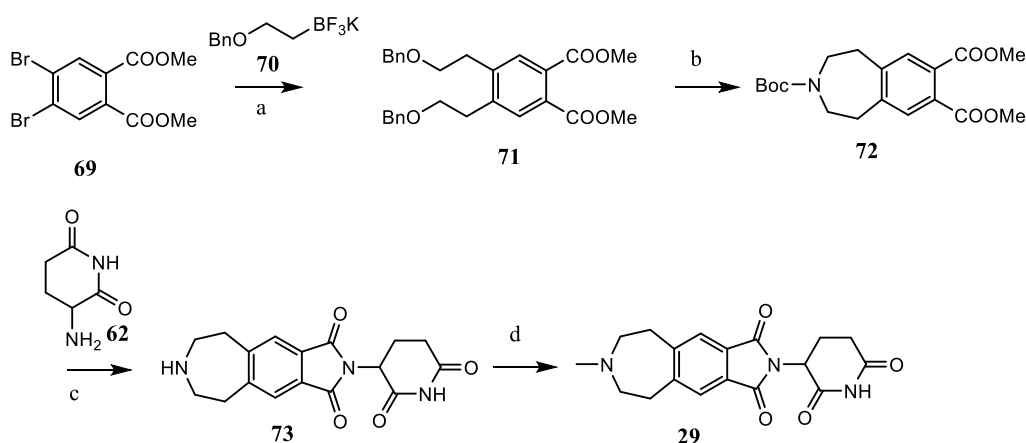
### Scheme 2. Synthesis of Cereblon Ligand 27<sup>a</sup>



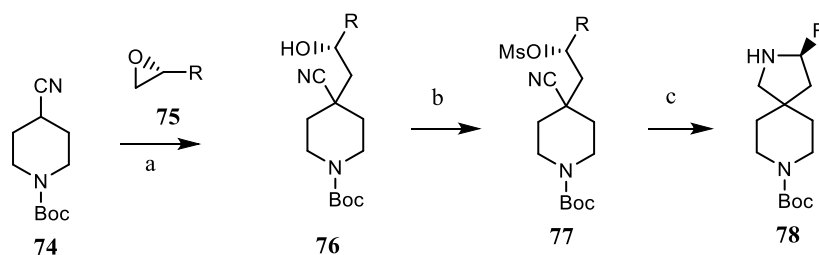
<sup>a</sup>Reaction conditions: (a) DMF, NaH, 0 °C, 3 h; (b) Wilkinson's catalyst, EtOH, reflux, overnight; (c) (1) LiI, PyH, reflux, 3 h; (2) DCM, TFA; (d) (1) formaldehyde, AcOH, NaB(AcO)<sub>3</sub>H; (2) DCM, TFA.

Scheme 3. Synthesis of Cereblon Ligand 28<sup>a</sup>

<sup>a</sup>Reaction conditions: (a) tetrakis(triphenylphosphine)palladium, NaOAc, dioxane, 110 °C, 24 h; (b) PtO<sub>2</sub>, EtOH, Boc<sub>2</sub>O; (c) (1) LiI, PyH, reflux, 3 h; (2) DCM, TFA; (d) (1) formaldehyde, AcOH, NaB(AcO)<sub>3</sub>H; (2) DCM, TFA.

Scheme 4. Synthesis of the Cereblon Ligand (29)<sup>a</sup>

<sup>a</sup>Reaction conditions: (a) tetrakis(triphenylphosphine)palladium, Cs<sub>2</sub>CO<sub>3</sub>, DMF; (b) (1) Pd/C, MeOH; (2) MsCl, TEA, DCM; (3) BnNH<sub>2</sub>, DIPEA, DMF; (4) Pd/C, Boc<sub>2</sub>O, MeOH; (c) (1) LiI, PyH, reflux, 3 h; (2) DCM, TFA; (d) (1) formaldehyde, AcOH, NaB(AcO)<sub>3</sub>H; (2) DCM, TFA.

Scheme 5. Synthesis of the S-Alkyl 5,6-Spiro Ring Intermediate (78)<sup>a</sup>

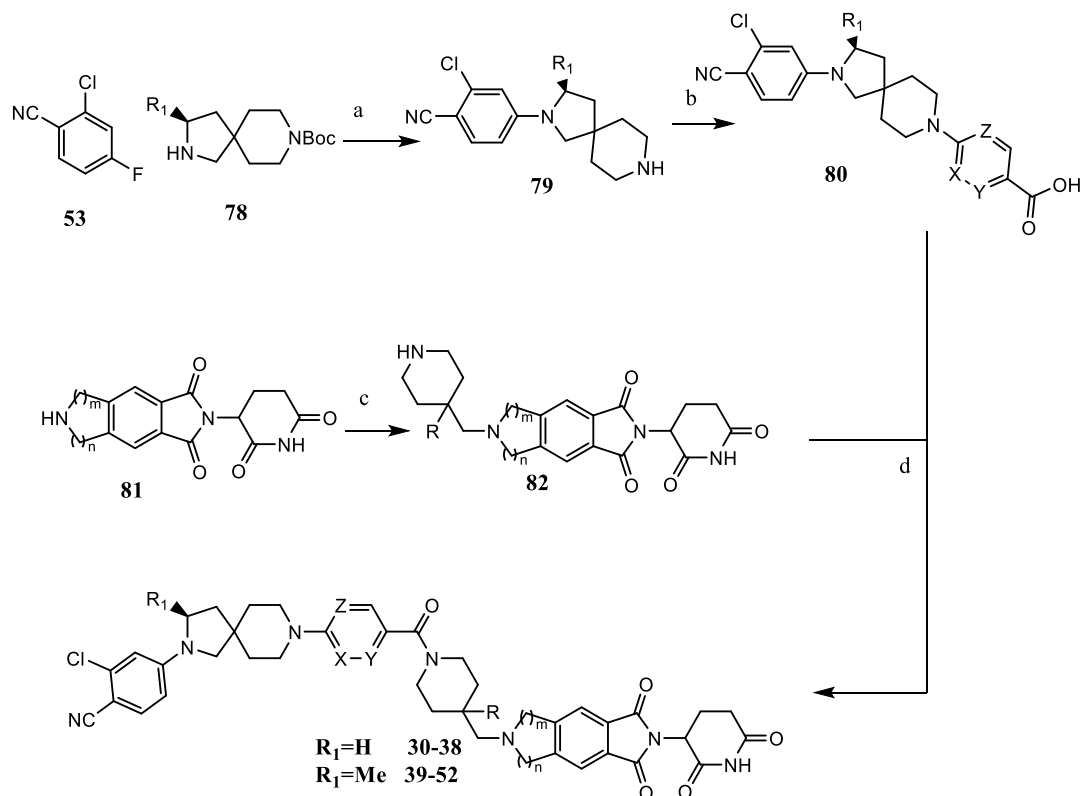
<sup>a</sup>Reaction conditions: (a) LDA, THF, -78 to 0 °C; (b) MsCl, TEA, DMAP, DCM, 0 °C; (c) LiAlH<sub>4</sub>, THF, rt.

mesylation of the resulting alcohol, cyclization with benzylamine, and change of the protecting group from benzyl to Boc with hydrogenation affords 72. The dicarboxylate (72) cyclizes with the amine in 62 to form 73 after deprotection of the Boc group. Methylation of the amine in 73 affords the cereblon ligand (29).

Sn<sub>2</sub> substitution of the carbocation in 74 with the epoxide (75) affords 76 (Scheme 5). Mesylation of the hydroxy group in 76 provides 77 and LiAlH<sub>4</sub> reduction of the cyano group in 77

followed by *in situ* Sn<sub>2</sub> substitution affords the 5,6-spiro compound (78).<sup>44</sup>

The synthesis of AR PROTACs (30–52) is shown in Scheme 6. Nucleophilic substitution of the fluoride in 53 with the amine in spiro 78, followed by deprotection of the Boc, affords the free amine compound (79). Buchwald coupling of amines in 79 with *tert*-butyl 4-iodobenzoate followed by TFA-assisted deprotection of the resulting *t*-butyl ester affords 80. Reductive amination of the cereblon ligand (81) with 4-formylpiperidine-1-Boc followed by deprotection of Boc affords 82. Amide coupling of

Scheme 6. Synthesis of AR PROTACs (30–52)<sup>a</sup>

<sup>a</sup>Reaction conditions: (a) (1) DMF, Cs<sub>2</sub>CO<sub>3</sub>, 110 °C, 16 h; (2) DCM, TFA; (b) (1) dioxane, *tert*-butyl 4-iodobenzoate, Pd<sub>2</sub>(dba)<sub>3</sub>, Xphos, Cs<sub>2</sub>CO<sub>3</sub>, 100 °C, 12 h; (2) DCM, TFA; (c) (1) aldehydes, AcOH, NaB(AcO)<sub>3</sub>H, 1,2-dichloroethane; (2) DCM, TFA; (d) HATU, DIPEA, DMF, rt, 0.5 h.

acid in **80** with the amines in **82** provides the AR PROTACs (**30–52**).

## SUMMARY

In this study, we sought to identify a new, highly potent, and orally active PROTAC AR degrader suitable for clinical development. For this purpose, we first designed a novel series of spiro ring system-based AR ligands and identified compound **23** as a high-binding-affinity AR ligand with IC<sub>50</sub> = 80 nM. We further designed three tricyclic cereblon ligands and identified the 5-membered ring fused tricyclic cereblon ligand **27** with a good affinity to cereblon. Employing AR ligand **23** and cereblon ligand **27**, we obtained compound **31** (ARD-1632) as a reasonably potent and effective AR degrader with DC<sub>50</sub> = 5.7 nM and D<sub>max</sub> of 88% in the VCaP cell line. Further optimization of the AR ligand portion in ARD-1632 led to the discovery of ARD-1676. ARD-1676 achieves DC<sub>50</sub> = 0.1 nM and D<sub>max</sub> of 99% in the VCaP cell line and DC<sub>50</sub> = 1.1 nM and D<sub>max</sub> of 98% in the LNCaP cell line. ARD-1676 potently inhibits cell growth with IC<sub>50</sub> = 11.5 and 2.8 nM, respectively, in these two AR+ prostate cancer cell lines. ARD-1676 effectively reduces the expression of AR-regulated PSA and TMPRSS2 genes with a potency >100-fold better than enzalutamide in both the VCaP and LNCaP cell lines. ARD-1676 selectively reduces the levels of the AR protein in the VCaP cell line among >5000 proteins in our proteomics analysis. Importantly, ARD-1676 effectively depletes the levels of a panel of clinically relevant AR mutant proteins at concentrations as low as 1 nM. ARD-1676 displays an excellent pharmacokinetic profile in rodent and non-rodent species and achieves an oral bioavailability (*F*) of 67, 44, 31, and 99% in

mice, rats, dogs, and monkeys, respectively. A single oral dose of ARD-1676 effectively depletes the AR protein in the VCaP tumor tissue, and daily, oral administration of ARD-1676 effectively inhibits tumor growth in the VCaP xenograft tumor model in mice without any sign of toxicity. Collectively, our data demonstrate that ARD-1676 is a highly promising development candidate for the treatment of advanced, AR+ human prostate cancer, as well as for other AR-dependent human diseases and conditions.

## EXPERIMENTAL SECTION

**Chemistry. General Information.** Unless otherwise specified, all purchased reagents were used as received without further purification. <sup>1</sup>H NMR and <sup>13</sup>C NMR spectra were recorded on a Bruker AVANCE 400 MHz spectrometer. <sup>1</sup>H NMR spectra are reported in parts per million (ppm) downfield from tetramethylsilane (TMS). All <sup>13</sup>C NMR spectra are reported in ppm and were obtained with <sup>1</sup>H decoupling. In reported spectral data, the format (δ) chemical shift (multiplicity, *J* values in Hz, integration) was used with the following abbreviations: s = singlet, d = doublet, t = triplet, q = quartet, and m = multiplet. Mass spectrometry (MS) analysis was conducted with a Waters ultra-performance liquid chromatography (UPLC) mass spectrometer. The final compounds were all purified by a C18 reverse-phase preparative high-performance liquid chromatography (HPLC) column with solvent A (0.1% TFA in H<sub>2</sub>O) and solvent B (0.1% TFA in CH<sub>3</sub>CN) as eluents. The purity of all of the final compounds was confirmed to be >95% by UPLC–MS and UPLC.

**2-Chloro-4-(2,8-diazaspiro[4.5]decan-2-yl)benzonitrile TFA Salt (55).** 2-Chloro-4-fluorobenzonitrile (1.54 g, 10 mmol, 1.0 equiv) and *tert*-butyl 2,8-diazaspiro[4.5]decan-8-carboxylate (1.92 g, 8 mmol, 0.8 equiv) were dissolved in DMF (15 mL), and Cs<sub>2</sub>CO<sub>3</sub> (9.75 g, 3.0 equiv) was added. The mixture was stirred at 120 °C overnight. The reaction

mixture was then cooled and partitioned between EtOAc and water. The organic layer was separated, washed with brine, dried, and purified with hexane and EtOAc using Combiflash to afford a white solid, which was dissolved in DCM (10 mL) and TFA (3 mL). The mixture was stirred at room temperature (rt) for 0.5 h. All the volatiles were removed in a rotary evaporator to provide 2.33 g of a light-yellow solid with a 75% yield. UPLC–MS: 3.8 min, purity > 95%, MS [M + H]<sup>+</sup>; found, 276.13, calcd, 276.12. <sup>1</sup>H NMR (MeCN-*d*<sub>3</sub>): δ 7.54 (d, *J* = 8.4 Hz, 1H), 7.04 (br, 2H), 6.70 (d, *J* = 2.4 Hz, 1H), 6.57 (dd, *J* = 8.8 Hz, 2.4 Hz, 1H), 3.47 (d, *J* = 6.8 Hz, 2H), 3.22 (m, 4H), 1.95 (m, 4H), 1.83 (m, 4H).

**4-(2-(3-Chloro-4-cyanophenyl)-2,8-diazaspiro[4.5]decan-8-yl)-benzoic Acid (56).** 2-Chloro-4-(2,8-diazaspiro[4.5]decan-2-yl)-benzonitrile (1.94 g, 5 mmol, 1.0 equiv), *t*-butyl 4-iodobenzoate (1.52 g, 5 mmol, 1.0 equiv), Pd<sub>2</sub>(dba)<sub>3</sub> (0.228 g, 0.05 equiv), Xphos (0.12 g, 0.05 equiv), and Cs<sub>2</sub>CO<sub>3</sub> (4.86 g, 3.0 equiv) were dissolved in dioxane (10 mL). The mixture was degassed and stirred at 110 °C overnight. The reaction mixture was cooled down and partitioned between EtOAc and water. The organic layer was separated, washed with water, dried, and purified with hexane and EtOAc using Combiflash to afford a solid, which was dissolved in DCM (10 mL) and TFA (5 mL). The mixture was stirred at rt for 2 h. All the volatiles were removed by a rotary evaporator to provide 1.58 g of a light-yellow solid with an 80% yield. UPLC–MS: 4.0 min, purity > 95%, MS [M + H]<sup>+</sup>; found, 396.18, calcd, 396.14. <sup>1</sup>H NMR (MeCN-*d*<sub>3</sub>): δ 7.92 ((d, *J* = 7.6 Hz, 2H), 7.53 (d, *J* = 8.8 Hz, 1H), 7.13 (d, *J* = 8.8 Hz, 2H), 6.70 (t, *J* = 2.4 Hz, 1H), 6.56 (dt, *J* = 8.8 Hz, 5.6 Hz, 1H), 3.46 (m, 6H), 3.29 (m, 2H), 3.17 (m, 2H), 1.82 (m, 4H).

**2-Chloro-4-(8-(4-(4-methylpiperazine-1-carbonyl)phenyl)-2,8-diazaspiro[4.5]decan-2-yl)benzonitrile (AR4034, 23).** Compound 56 (0.395 g, 1 mmol, 1.0 equiv), DIPEA (0.39 g, 3.0 equiv), and HATU (0.495 g, 1.3 equiv) were dissolved in DCM (10 mL) and stirred at rt for 15 min. *N*-Methyl piperazine (0.11 g, 1.1 equiv) was added, and the reaction was completed in 0.5 h. The reaction mixture was concentrated, acidified with TFA, and purified by prep-HPLC to provide the target compound in a 90% yield as a white solid. UPLC–MS: 4.5 min, purity > 95%, MS [M + H]<sup>+</sup>; found, 478.21, calcd, 478.23. Prep. HPLC 46% MeCN in water. <sup>1</sup>H NMR (MeCN-*d*<sub>3</sub>): δ 10.95 (br, 1H), 7.52 (d, *J* = 8.8 Hz, 1H), 7.43 (d, *J* = 8.4 Hz, 2H), 7.15 (d, *J* = 6.8 Hz, 2H), 6.71 (d, *J* = 2.0 Hz, 1H), 6.57 (dd, *J* = 9.6 Hz, 2.4 Hz, 1H), 5.05 (m, 4H), 4.29 (m, 2H), 4.34 (m, 2H), 3.47 (m, 6H), 3.31 (m, 4H), 3.00 (m, 2H), 2.82 (s, 3H), 1.82 (m, 2H).

**2-(2,6-Dioxopiperidin-3-yl)-6,7-dihydropyrrolo[3,4-*f*]isoindole-1,3(2*H*,5*H*)-dione TFA Salt (63).** 2-(*tert*-Butyl) 5,6-dimethyl isoindoline-2,5,6-tricarboxylate (0.335 g, 1 mmol, 1.0 equiv), 3-amino-piperidine-2,6-dione<sup>41</sup> (0.165 g, 1.3 equiv), and KI (3.0 equiv) were dissolved in pyridine (1.58 g, 20.0 equiv) and refluxed overnight. The reaction mixture was cooled to rt and then concentrated under vacuum. The residue was purified by DCM and MeOH using Combiflash to give a white solid, which was dissolved in DCM (10 mL) and TFA (3 mL). The mixture was stirred at rt for 0.5 h. All the volatiles were removed in a rotary evaporator to provide a pale solid with a 65% yield. UPLC–MS: 1.0 min, purity > 95%, MS [M + H]<sup>+</sup>; found, 300.08, calcd, 300.09. <sup>1</sup>H NMR (DMSO-*d*<sub>6</sub>): δ 10.30 (br, 1H), 9.06 (s, 1H), 7.13 (s, 2H), 4.35 (m, 1H), 3.83 (s, 4H), 2.06 (m, 1H), 1.79 (m, 1H), 1.68 (m, 1H), 1.25 (m, 1H).

**2-(2,6-Dioxopiperidin-3-yl)-6-methyl-6,7-dihydropyrrolo[3,4-*f*]isoindole-1,3(2*H*,5*H*)-dione TFA Salt (27).** 2-(2,6-Dioxopiperidin-3-yl)-6,7-dihydropyrrolo[3,4-*f*]isoindole-1,3(2*H*,5*H*)-dione (0.15 g, 0.5 mmol, 1.0 equiv) was dissolved in 1,2-dichloroethane (5 mL), and formaldehyde (0.081 g, 2.0 equiv, 37% in water) and AcOH (0.09 g, 3.0 equiv) were added. After stirring for 0.5 h, NaB(AcO)<sub>3</sub>H (0.318 g, 3.0 equiv) was added. UPLC–MS showed that the reaction was complete in 2 h. The reaction mixture was purified by Combiflash with DCM and MeOH to give a white solid. The resulting solid was dissolved in DCM (10 mL) and TFA (2 mL). After 2 h, all volatiles were removed, and the residue was purified by prep-HPLC to afford the title compound in a 65% yield. UPLC–MS: 1.2 min, purity > 95%, MS [M + H]<sup>+</sup>; found, 314.13, calcd, 314.11. Prep. HPLC 16% MeCN in water. <sup>1</sup>H NMR

(MeCN-*d*<sub>3</sub>): δ 9.09 (s, 1H), 7.99 (br, 1H), 7.85 (s, 2H), 5.20 (m, 1H), 5.03 (m, 2H), 4.56 (m, 2H), 3.09 (s, 3H), 2.78 (m, 3H), 2.19 (m, 1H).

**2-(2,6-Dioxopiperidin-3-yl)-5,6,7,8-tetrahydro-1*H*-pyrrolo[3,4-*g*]isoquinoline-1,3(2*H*)-dione (68).** The title compound was synthesized in a 75% yield from the intermediate 2-(*tert*-butyl)-6,7-dimethyl 3,4-dihydroisoquinoline-2,6,7(1*H*)-tricarboxylate<sup>42</sup> following the procedure used for the 5-membered ring tricyclic cereblon ligand. UPLC–MS: 1.0 min, purity > 95%, MS [M + H]<sup>+</sup>; found, 314.15, calcd, 314.11. <sup>1</sup>H NMR (DMSO-*d*<sub>6</sub>): δ 10.45 (br, 1H), 8.69 (s, 2H), 7.18 (d, *J* = 6.8 Hz, 2H), 4.45 (m, 1H), 3.80 (m, 2H), 2.77 (m, 2H), 2.50 (m, 2H), 2.21 (m, 1H), 1.95 (m, 2H), 1.41 (m, 1H).

**2-(2,6-Dioxopiperidin-3-yl)-6-methyl-5,6,7,8-tetrahydro-1*H*-pyrrolo[3,4-*g*]isoquinoline-1,3(2*H*)-dione TFA Salt (28).** The title compound was synthesized in a 60% yield following the procedure used for the cereblon ligand (24). UPLC–MS: 1.3 min, purity > 95%, MS [M + H]<sup>+</sup>; found, 328.16, calcd, 328.12. Prep. HPLC 17% MeCN in water. <sup>1</sup>H NMR (MeCN-*d*<sub>3</sub>): δ 9.06 (s, 1H), 7.77 (s, 1H), 7.69 (s, 1H), 7.25 (br, 1H), 5.18 (m, 1H), 5.06 (m, 1H), 4.67 (m, 1H), 4.36 (m, 1H), 3.73 (m, 1H), 3.37 (m, 2H), 2.99 (s, 3H), 2.86 (m, 1H), 2.75 (m, 2H), 2.18 (m, 1H).

**2-(2,6-Dioxopiperidin-3-yl)-6,7,8,9-tetrahydroazepino[4,5-*f*]isoindole-1,3(2*H*,5*H*)-dione TFA Salt (73).** The title compound was synthesized from known intermediate 3-(*tert*-butyl) 7,8-dimethyl 1,2,4,5-tetrahydro-3*H*-benzo[*d*]azepine-3,7,8-tricarboxylate<sup>43</sup> following the procedure used for preparation of the 5-membered ring tricyclic cereblon ligand in a 70% yield. UPLC–MS: 1.4 min, purity > 95%, MS [M + H]<sup>+</sup>; found, 328.17, calcd, 328.12. <sup>1</sup>H NMR (DMSO-*d*<sub>6</sub>): δ 10.26 (br, 1H), 8.82 (s, 2H), 6.95 (s, 2H), 4.30 (m, 1H), 2.71 (m, 4H), 2.51 (m, 1H), 2.08 (m, 4H), 2.01 (m, 1H), 1.73 (m, 2H), 1.23 (m, 1H).

**2-(2,6-Dioxopiperidin-3-yl)-7-methyl-6,7,8,9-tetrahydroazepino[4,5-*f*]isoindole-1,3(2*H*,5*H*)-dione TFA Salt (29).** The title compound was synthesized following the procedure used to prepare the cereblon ligand (24) in a 60% yield. UPLC–MS: 1.6 min, purity > 95%, MS [M + H]<sup>+</sup>; found, 342.20, calcd, 342.14. Prep. HPLC 19% MeCN in water. <sup>1</sup>H NMR (MeCN-*d*<sub>3</sub>): δ 9.08 (s, 1H), 7.71 (s, 2H), 7.73 (s, 1H), 5.18 (m, 1H), 5.06 (m, 1H), 3.69 (m, 2H), 3.49 (s, 2H), 3.28 (m, 2H), 3.01 (m, 2H), 2.88 (s, 3H), 2.71 (m, 2H), 2.16 (m, 1H).

**2-Chloro-4-(8-(4-(4-(6-(2,6-dioxopiperidin-3-yl)-5,7-dioxo-3,5,6,7-tetrahydropyrrolo[3,4-*f*]isoindol-2(1*H*)-yl)piperidine-1-carbonyl)phenyl)-2,8-diazaspiro[4.5]decan-2-yl)benzonitrile (30).** Step 1: 2-(2,6-Dioxopiperidin-3-yl)-6-(piperidin-4-yl)-6,7-dihydropyrrolo[3,4-*f*]isoindole-1,3(2*H*,5*H*)-dione TFA salt.

2-(2,6-Dioxopiperidin-3-yl)-6,7-dihydropyrrolo[3,4-*f*]isoindole-1,3(2*H*,5*H*)-dione (0.30 g, 1 mmol, 1.0 equiv), *N*-Boc 4-piperidone (0.3 g, 1.5 equiv), and AcOH (0.18 g, 3.0 equiv) were dissolved in 1,2-dichloroethane (3 mL), and 4 Å molecular sieves (0.3 g) were added to the solution. The NaB(AcO)<sub>3</sub>H (0.636 g, 3.0 equiv) was added, and the mixture was stirred overnight, completing the reaction in 2 h. The reaction mixture was directly placed on a silica gel column of Combiflash and purified with DCM and MeOH to give a white solid, which was dissolved in DCM (10 mL) and TFA (2 mL). After 0.5 h, all volatiles were removed and dried to give the title compound in a 60% yield. UPLC–MS: 1.6 min, purity > 95%, MS [M + H]<sup>+</sup>; found, 383.12, calcd, 383.16. <sup>1</sup>H NMR (MeCN-*d*<sub>3</sub>): δ 8.96 (s, 2H), 8.41 (br, 2H), 7.84 (s, 2H), 5.08 (m, 1H), 4.77 (m, 4H), 3.54 (m, 4H), 3.05 (m, 2H), 2.76 (m, 3H), 2.35 (m, 1H), 2.16 (m, 3H).

Step 2: 2-Chloro-4-(8-(4-(4-(6-(2,6-dioxopiperidin-3-yl)-5,7-dioxo-3,5,6,7-tetrahydropyrrolo[3,4-*f*]isoindol-2(1*H*)-yl)piperidine-1-carbonyl)phenyl)-2,8-diazaspiro[4.5]decan-2-yl)benzonitrile (ARD-1631, 30).

**4-(2-(3-Chloro-4-cyanophenyl)-2,8-diazaspiro[4.5]decan-8-yl)-benzoic acid (0.198 g, 0.5 mmol, 1.0 equiv), DIPEA (0.195 g, 3.0 equiv), and HATU (0.245 g, 0.65 mmol, 1.3 equiv) were dissolved in DMF (3 mL). To the above mixture, the intermediate 2-(2,6-dioxopiperidin-3-yl)-6-(piperidin-4-yl)-6,7-dihydropyrrolo[3,4-*f*]isoindole-1,3(2*H*,5*H*)-dione TFA salt (0.28 g, 0.55 mmol, 1.1 equiv) and DIPEA (0.195 g, 3.0 equiv) in DMF (2 mL) were added. The reaction was finished in 0.5 h. The reaction mixture was acidified and purified by prep-HPLC to give the titled compound in a 70% yield.**

UPLC–MS: 4.4 min, purity > 95%, MS [M + H]<sup>+</sup>; found, 760.24, calcd, 760.29. Prep. HPLC 36% MeCN in water. <sup>1</sup>H NMR (MeCN-*d*<sub>3</sub>): δ 8.95 (br, 1H), 7.84 (s, 2H), 7.52 (d, J = 8.8 Hz, 1H), 7.37 (d, J = 8.8 Hz, 2H), 7.08 (d, J = 8.4 Hz, 2H), 6.71 (d, J = 2.4 Hz, 1H), 6.57 (dd, J = 8.8 Hz, 2.4 Hz, 1H), 5.08 (m, 1H), 4.82 (m, 3H), 4.34 (m, 2H), 3.65 (m, 2H), 3.46 (m, 3H), 3.30 (m, 2H), 2.98 (m, 2H), 2.77 (m, 3H), 2.16 (m, 2H), 1.98 (m, 8H), 1.78 (m, 4H).

**2-Chloro-4-(8-(4-(4-((6-(2,6-dioxopiperidin-3-yl)-5,7-dioxo-3,5,6,7-tetrahydropyrrolo[3,4-*f*]isoindol-2(1H)-yl)methyl)piperidine-1-carbonyl)phenyl)-2,8-diazaspiro[4.5]decan-2-yl)benzonitrile (ARD-1632, 31).** UPLC–MS: 4.4 min, purity > 95%, MS [M + H]<sup>+</sup>; found, 774.35, calcd, 774.31. Prep. HPLC 36% MeCN in water. <sup>1</sup>H NMR (MeCN-*d*<sub>3</sub>): δ 8.95 (br, 1H), 7.83 (s, 2H), 7.52 (d, J = 8.8 Hz, 1H), 7.34 (d, J = 8.8 Hz, 2H), 7.00 (d, J = 8.4 Hz, 2H), 6.71 (d, J = 2.4 Hz, 1H), 6.57 (dd, J = 8.8 Hz, 2.0 Hz, 1H), 5.03 (m, 1H), 4.45 (m, 1H), 4.21 (m, 1H), 3.34 (m, 4H), 3.29 (m, 4H), 2.98 (m, 3H), 2.76 (m, 4H), 2.14 (m, 4H), 2.02 (m, 2H), 1.92 (m, 2H), 1.80 (m, 2H), 1.73 (m, 2H), 1.35 (m, 4H).

**2-Chloro-4-(8-(4-(4-(2-(6-(2,6-dioxopiperidin-3-yl)-5,7-dioxo-3,5,6,7-tetrahydropyrrolo[3,4-*f*]isoindol-2(1H)-yl)ethyl)piperidine-1-carbonyl)phenyl)-2,8-diazaspiro[4.5]decan-2-yl)benzonitrile (ARD-1633, 32).** UPLC–MS: 4.5 min, purity > 95%, MS [M + H]<sup>+</sup>; found, 788.35, calcd, 788.32. Prep. HPLC 38% MeCN in water. <sup>1</sup>H NMR (MeCN-*d*<sub>3</sub>): δ 8.95 (br, 1H), 7.83 (s, 2H), 7.52 (d, J = 8.8 Hz, 1H), 7.32 (d, J = 8.8 Hz, 2H), 7.00 (d, J = 9.2 Hz, 2H), 6.70 (d, J = 2.0 Hz, 1H), 6.57 (dd, J = 9.2 Hz, 2.4 Hz, 1H), 5.02 (m, 1H), 4.21 (m, 2H), 3.42 (m, 4H), 3.29 (m, 4H), 3.16 (m, 2H), 2.76 (m, 2H), 2.68 (m, 4H), 2.13 (m, 4H), 2.02 (m, 3H), 1.92 (m, 1H), 1.80 (m, 2H), 1.75 (m, 2H), 1.35 (m, 5H).

**2-Chloro-4-(8-(4-(4-(2-(6-(2,6-dioxopiperidin-3-yl)-1,3-dioxo-1,2,3,5,7,8-hexahydro-6H-pyrrolo[3,4-*g*]isoquinolin-6-yl)piperidine-1-carbonyl)phenyl)-2,8-diazaspiro[4.5]decan-2-yl)benzonitrile (ARD-1628, 33).** UPLC–MS: 4.5 min, purity > 95%, MS [M + H]<sup>+</sup>; found, 774.30, calcd, 774.31. Prep. HPLC 41% MeCN in water. <sup>1</sup>H NMR (MeCN-*d*<sub>3</sub>): δ 8.94 (br, 1H), 7.87 (d, J = 8.8 Hz, 1H), 7.77 (s, 1H), 7.54 (d, J = 8.8 Hz, 1H), 7.50 (d, J = 8.8 Hz, 1H), 7.35 (d, J = 8.8 Hz, 1H), 7.03 (d, J = 9.2 Hz, 1H), 6.81 (d, J = 9.2 Hz, 1H), 6.71 (d, J = 2.4 Hz, 1H), 6.65 (dd, J = 8.8 Hz, 2.4 Hz, 1H), 5.02 (m, 1H), 4.45 (m, 1H), 3.87 (m, 2H), 3.70 (m, 3H), 3.45 (m, 4H), 3.28 (m, 4H), 3.16 (m, 3H), 2.78 (m, 4H), 2.13 (m, 2H), 2.05 (m, 2H), 1.89 (m, 2H), 1.81 (m, 2H), 1.76 (m, 3H), 1.65 (m, 1H).

**2-Chloro-4-(8-(4-(4-(2-(6-(2,6-dioxopiperidin-3-yl)-1,3-dioxo-1,2,3,5,7,8-hexahydro-6H-pyrrolo[3,4-*g*]isoquinolin-6-yl)methyl)piperidine-1-carbonyl)phenyl)-2,8-diazaspiro[4.5]decan-2-yl)benzonitrile (ARD-1629, 34).** UPLC–MS: 4.5 min, purity > 95%, MS [M + H]<sup>+</sup>; found, 788.29, calcd, 788.32. Prep. HPLC 41% MeCN in water. <sup>1</sup>H NMR (MeCN-*d*<sub>3</sub>): δ 8.94 (br, 1H), 7.76 (s, 1H), 7.70 (s, 1H), 7.52 (d, J = 8.8 Hz, 1H), 7.34 (d, J = 8.8 Hz, 2H), 7.03 (d, J = 8.8 Hz, 2H), 6.70 (d, J = 2.4 Hz, 1H), 6.57 (dd, J = 9.2 Hz, 2.4 Hz, 1H), 5.01 (m, 2H), 4.21 (m, 2H), 3.85 (m, 1H), 3.76 (m, 1H), 3.43 (m, 6H), 3.26 (m, 4H), 3.14 (m, 4H), 2.28 (m, 2H), 2.13 (m, 2H), 2.05 (m, 2H), 1.91 (m, 1H), 1.87 (m, 1H), 1.74 (m, 4H), 1.65 (m, 4H).

**2-Chloro-4-(8-(4-(4-(2-(2-(2,6-dioxopiperidin-3-yl)-1,3-dioxo-1,2,3,5,7,8-hexahydro-6H-pyrrolo[3,4-*g*]isoquinolin-6-yl)ethyl)piperidine-1-carbonyl)phenyl)-2,8-diazaspiro[4.5]decan-2-yl)benzonitrile (ARD-1630, 35).** UPLC–MS: 4.6 min, purity > 95%, MS [M + H]<sup>+</sup>; found, 802.28, calcd, 802.34. Prep. HPLC 42% MeCN in water. <sup>1</sup>H NMR (MeCN-*d*<sub>3</sub>): δ 8.94 (br, 1H), 7.80 (dd, J = 8.8 Hz, 2.0 Hz, 1H), 7.70 (s, 1H), 7.52 (d, J = 8.8 Hz, 1H), 7.33 (dd, J = 8.8 Hz, 1.2 Hz, 2H), 7.00 (dd, J = 9.2 Hz, 4.0 Hz, 2H), 6.70 (d, J = 2.4 Hz, 1H), 6.57 (dd, J = 8.8 Hz, 2.4 Hz, 1H), 5.03 (m, 1H), 4.45 (m, 1H), 3.85 (m, 1H), 3.75 (m, 2H), 3.57 (m, 1H), 3.46 (m, 3H), 3.27 (m, 4H), 3.02 (m, 2H), 2.89 (m, 3H), 2.72 (m, 2H), 2.16 (m, 4H), 1.84 (m, 4H), 1.73 (m, 2H), 1.56 (m, 2H), 1.44 (m, 2H), 1.31 (m, 2H), 1.16 (m, 2H).

**2-Chloro-4-(8-(4-(4-(2-(2-(2,6-dioxopiperidin-3-yl)-1,3-dioxo-2,3,5,6,8,9-hexahydroazepino[4,5-*f*]isoindol-7(1H)-yl)piperidine-1-carbonyl)phenyl)-2,8-diazaspiro[4.5]decan-2-yl)benzonitrile (ARD-4050, 36).** UPLC–MS: 4.6 min, purity > 95%, MS [M + H]<sup>+</sup>; found, 788.28, calcd, 788.32. Prep. HPLC 42% MeCN in water. <sup>1</sup>H NMR (MeCN-*d*<sub>3</sub>): δ 8.97 (br, 1H), 7.69 (s, 2H), 7.50 (d, J = 8.4 Hz, 1H), 7.32 (d, J = 8.4 Hz, 2H), 7.11 (d, J = 9.2 Hz, 2H), 6.82 (d, J = 2.4 Hz, 1H), 6.63 (dd, J = 8.8 Hz, 2.0 Hz, 1H), 5.04 (m, 1H), 3.65 (m, 3H), 3.47 (m,

3H), 3.29 (m, 4H), 3.05 (m, 6H), 2.99 (m, 4H), 2.75 (m, 4H), 2.22 (m, 4H), 1.86 (m, 4H), 1.30 (m, 3H).

**2-Chloro-4-(8-(4-(4-(2-(2-(2,6-dioxopiperidin-3-yl)-1,3-dioxo-2,3,5,6,8,9-hexahydroazepino[4,5-*f*]isoindol-7(1H)-yl)methyl)piperidine-1-carbonyl)phenyl)-2,8-diazaspiro[4.5]decan-2-yl)benzonitrile (ARD-4051, 37).** UPLC–MS: 4.7 min, purity > 95%, MS [M + H]<sup>+</sup>; found, 802.27, calcd, 802.34. Prep. HPLC 43% MeCN in water. <sup>1</sup>H NMR (MeCN-*d*<sub>3</sub>): δ 8.95 (br, 1H), 7.72 (s, 2H), 7.52 (d, J = 8.8 Hz, 1H), 7.30 (d, J = 8.8 Hz, 2H), 7.01 (d, J = 8.8 Hz, 2H), 6.71 (d, J = 2.4 Hz, 1H), 6.57 (dd, J = 8.8 Hz, 2.0 Hz, 1H), 5.02 (m, 1H), 3.77 (m, 2H), 3.63 (m, 2H), 3.45 (m, 3H), 3.27 (m, 5H), 3.04 (m, 5H), 2.96 (m, 5H), 2.74 (m, 4H), 2.20 (m, 3H), 2.03 (m, 1H), 1.90 (m, 1H), 1.75 (m, 3H), 1.33 (m, 3H).

**2-Chloro-4-(8-(4-(4-(2-(2-(2,6-dioxopiperidin-3-yl)-1,3-dioxo-2,3,5,6,8,9-hexahydroazepino[4,5-*f*]isoindol-7(1H)-yl)ethyl)piperidine-1-carbonyl)phenyl)-2,8-diazaspiro[4.5]decan-2-yl)benzonitrile (ARD-4052, 38).** UPLC–MS: 5.0 min, purity > 95%, MS [M + H]<sup>+</sup>; found, 816.21, calculated 816.36. Prep. HPLC 47% MeCN in water. <sup>1</sup>H NMR (MeCN-*d*<sub>3</sub>): δ 8.95 (br, 1H), 7.72 (s, 2H), 7.52 (d, J = 8.8 Hz, 1H), 7.32 (d, J = 8.8 Hz, 2H), 6.98 (d, J = 8.8 Hz, 2H), 6.70 (d, J = 2.4 Hz, 1H), 6.57 (dd, J = 8.8 Hz, 2.4 Hz, 1H), 5.02 (m, 1H), 3.76 (m, 2H), 3.60 (m, 2H), 3.42 (m, 2H), 3.29 (m, 3H), 3.15 (m, 3H), 2.91 (m, 5H), 2.75 (m, 5H), 2.16 (m, 2H), 2.01 (m, 2H), 1.75 (m, 6H), 1.38 (m, 7H).

Synthesis of 2-chloro-4-((3S)-8-(4-(4-((6-(2,6-dioxopiperidin-3-yl)-5,7-dioxo-3,5,6,7-tetrahydropyrrolo[3,4-*f*]isoindol-2(1H)-yl)-methyl)piperidine-1-carbonyl)phenyl)-3-methyl-2,8-diazaspiro[4.5]decan-2-yl)benzonitrile TFA salt (ARD-1676, 39).

**Step 1: (S)-2-Chloro-4-(3-methyl-2,8-diazaspiro[4.5]decan-2-yl)benzonitrile.** 2-Chloro-4-fluorobenzonitrile (1.55 g, 10 mmol, 1.0 equiv) and the intermediate *tert*-butyl (S)-3-methyl-2,8-diazaspiro[4.5]decan-8-carboxylate (2.03 g, 8 mmol, 0.8 equiv) were dissolved in DMF (15 mL), and Cs<sub>2</sub>CO<sub>3</sub> (9.78 g, 3.0 equiv) was added. The mixture was stirred at 120 °C overnight. The reaction mixture was cooled and partitioned between EtOAc and water. The organic layer was separated, washed with brine, dried, and purified with hexane and EtOAc using Combiflash to afford a white solid, which was dissolved in DCM (10 mL) and TFA (3 mL). The mixture was stirred at rt for 0.5 h. All the volatiles were removed by a rotary evaporator to provide a light-yellow solid with a 70% yield. UPLC–MS: 4.0 min, purity > 95%, MS [M + H]<sup>+</sup>; found, 290.10, calcd, 290.13. <sup>1</sup>H NMR (MeCN-*d*<sub>3</sub>): δ 8.98 (br, 2H), 7.52 (d, J = 8.8 Hz, 1H), 6.75 (d, J = 2.4 Hz, 1H), 6.61 (dd, J = 8.8 Hz, 2.4 Hz, 1H), 4.04 (m, 1H), 3.42 (m, 2H), 3.14 (m, 4H), 2.34 (m, 1H), 2.16 (m, 2H), 1.76 (m, 2H), 1.68 (m, 1H), 1.25 (d, J = 6.0 Hz, 3H).

**Step 2: (S)-4-(2-(3-Chloro-4-cyanophenyl)-3-methyl-2,8-diazaspiro[4.5]decan-8-yl)benzoic Acid.** The intermediate (S)-2-chloro-4-(3-methyl-2,8-diazaspiro[4.5]decan-2-yl)benzonitrile TFA salt (2.02 g, 5 mmol, 1.0 equiv), *t*-butyl 4-iodobenzoate (1.52 g, 5 mmol, 1.0 equiv), Pd<sub>2</sub>(dba)<sub>3</sub> (0.229 g, 0.25 mmol, 0.05 equiv), Xphos (0.119 g, 0.05 mmol, 0.05 equiv), and Cs<sub>2</sub>CO<sub>3</sub> (4.86 g, 3.0 equiv) were dissolved in dioxane (20 mL). The mixture was degassed and stirred at 110 °C overnight. The reaction mixture was cooled down and partitioned between EtOAc and water. The organic layer was separated, washed with water, dried, and purified with hexane and EtOAc using Combiflash to afford a solid, which was dissolved in DCM (10 mL) and TFA (5 mL). The mixture was stirred at rt for 2 h. All the volatiles were removed in a rotary evaporator to provide 1.58 g of a light-yellow solid with an 80% yield. UPLC–MS: 4.1 min, purity > 95%, MS [M + H]<sup>+</sup>; found, 410.10, calcd, 410.16. <sup>1</sup>H NMR (MeCN-*d*<sub>3</sub>): δ 7.86 (dd, J = 7.2 Hz, 2.0 Hz, 2H), 7.51 (d, J = 8.8 Hz, 1H), 6.96 (d, J = 6.8 Hz, 2H), 6.75 (d, J = 3.2 Hz, 1H), 6.61 (dd, J = 8.8 Hz, 2.4 Hz, 1H), 4.05 (m, 1H), 3.47 (m, 2H), 3.37 (m, 2H), 2.30 (m, 2H), 1.79 (m, 2H), 1.73 (m, 2H), 1.27 (m, 2H), 1.16 (m, 3H).

**Step 3: 2-(2,6-Dioxopiperidin-3-yl)-6-(piperidin-4-ylmethyl)-6,7-dihydropyrrolo[3,4-*f*]isoindole-1,3(2H,5H)-dione TFA Salt.** 2-(2,6-Dioxopiperidin-3-yl)-6,7-dihydropyrrolo[3,4-*f*]isoindole-1,3(2H,5H)-dione (0.15 g, 0.5 mmol, 1.0 equiv), *tert*-butyl 4-formylpiperidine-1-carboxylate (0.15 g, 0.75 mmol, 1.5 equiv), and NaOAc (0.246 g, 3.0 equiv) were dissolved in MeOH (4 mL). After 15 min, NaBCNH<sub>3</sub> (0.3 g, 3.0 equiv) was added. The reaction was completed in 1 h. All volatiles

were removed, and the residue was purified by Combiflash with DCM and MeOH to give a white solid, which was dissolved in DCM (3 mL) and TFA (1 mL). After 0.5 h, all volatiles were removed and dried to give the title compound in an 80% yield. UPLC–MS: 1.7 min, purity > 95%, MS [M + H]<sup>+</sup>; found, 397.13, calcd, 397.18. <sup>1</sup>H NMR (MeCN-*d*<sub>3</sub>): δ 8.96 (s, 2H), 7.86 (s, 2H), 7.12 (br, 2H), 5.04 (m, 1H), 4.81 (m, 4H), 3.46 (m, 2H), 3.35 (m, 2H), 3.01 (m, 2H), 2.79 (m, 2H), 2.18 (m, 2H), 2.01 (m, 2H), 1.62 (m, 2H), 1.34 (m, 1H).

**Step 4:** 2-Chloro-4-((3*S*)-8-(4-(4-((6-(2,6-dioxopiperidin-3-yl)-5,7-dioxo-3,5,6,7-tetrahydropyrrolo[3,4-*f*]isoindol-2(1*H*)-yl)methyl)piperidine-1-carbonyl)phenyl)-3-methyl-2,8-diazaspiro[4.5]decan-2-yl)benzonitrile TFA Salt (ARD-1676, 39). (S)-4-(2-(3-Chloro-4-cyanophenyl)-3-methyl-2,8-diazaspiro[4.5]decan-8-yl)benzoic acid (0.082 g, 0.2 mmol, 1.0 equiv), DIPEA (0.078 g, 3.0 equiv), and HATU (0.099 g, 1.3 equiv) were dissolved in DMF (2 mL). To the above mixture, 2-(2,6-dioxopiperidin-3-yl)-6-(piperidin-4-ylmethyl)-6,7-dihydropyrrolo[3,4-*f*]isoindole-1,3(2*H*,5*H*)-dione TFA salt (0.11 g, 0.22 mmol, 1.1 equiv) and DIPEA (0.078 g, 3.0 equiv) in DMF (1 mL) were added. The reaction was completed in 0.5 h. The reaction mixture was acidified and purified by prep-HPLC to give the titled compound in a 70% yield. UPLC–MS: 4.6 min, purity > 95%, MS [M + H]<sup>+</sup>; found, 788.30, calcd, 788.32. Prep. HPLC 38% MeCN in water. <sup>1</sup>H NMR (DMSO-*d*<sub>6</sub>): δ 12.17 (br, 1H), 11.14 (s, 1H), 7.96 (s, 2H), 7.62 (d, *J* = 8.8 Hz, 1H), 7.43 (m, 3H), 6.82 (d, *J* = 2.4 Hz, 1H), 6.70 (dd, *J* = 9.6 Hz, 2.4 Hz, 1H), 6.61 (dd, *J* = 8.8 Hz, 2.4 Hz, 1H), 5.51 (m, 1H), 5.02 (m, 2H), 4.70 (m, 2H), 4.07 (m, 2H), 3.93 (m, 6H), 3.57 (m, 1H), 3.47 (m, 3H), 2.90 (m, 3H), 2.59 (m, 2H), 2.31 (m, 1H), 2.15 (m, 2H), 1.95 (m, 3H), 1.79 (m, 1H), 1.66 (m, 2H), 1.27 (m, 2H), 1.21 (d, 3H). <sup>13</sup>C NMR (DMSO-*d*<sub>6</sub>): δ 173.2, 170.2, 169.1, 167.0, 151.2, 142.3, 136.9, 135.1, 132.2, 128.9, 118.7, 118.3, 113.0, 112.0, 96.2, 66.8, 59.6, 58.4, 52.9, 49.7, 34.1, 33.5, 33.0, 31.4, 30.1, 22.5, 19.9.

**2-Chloro-4-((3*R*)-8-(4-(4-((6-(2,6-dioxopiperidin-3-yl)-5,7-dioxo-3,5,6,7-tetrahydropyrrolo[3,4-*f*]isoindol-2(1*H*)-yl)methyl)piperidine-1-carbonyl)phenyl)-3-methyl-2,8-diazaspiro[4.5]decan-2-yl)benzonitrile (ARD-1719, 40).** UPLC–MS: 4.6 min, purity > 95%, MS [M + H]<sup>+</sup>; found, 788.31, calcd, 788.32. Prep. HPLC 38% MeCN in water. <sup>1</sup>H NMR (MeCN-*d*<sub>3</sub>): δ 8.95 (br, 1H), 7.83 (s, 2H), 7.51 (d, *J* = 8.8 Hz, 1H), 7.33 (dd, *J* = 6.4 Hz, 2.0 Hz, 2H), 7.00 (d, *J* = 8.8 Hz, 2H), 6.76 (d, *J* = 2.4 Hz, 1H), 6.64 (dd, *J* = 8.8 Hz, 2.4 Hz, 1H), 5.07 (m, 1H), 4.79 (m, 4H), 4.21 (m, 2H), 4.05 (m, 1H), 3.41 (m, 4H), 3.23 (m, 4H), 2.97 (m, 3H), 2.76 (m, 4H), 2.30 (m, 1H), 2.20 (m, 2H), 2.01 (m, 1H), 1.92 (m, 2H), 1.83 (m, 1H), 1.63 (m, 2H), 1.32 (m, 1H), 1.21 (m, 3H).

**2-Chloro-4-((3*S*)-8-(4-(4-((6-(2,6-dioxopiperidin-3-yl)-5,7-dioxo-3,5,6,7-tetrahydropyrrolo[3,4-*f*]isoindol-2(1*H*)-yl)methyl)piperidine-1-carbonyl)phenyl)-3-ethyl-2,8-diazaspiro[4.5]decan-2-yl)benzonitrile (ARD-1693, 41).** UPLC–MS: 4.7 min, purity > 95%, MS [M + H]<sup>+</sup>; found, 802.31, calcd, 802.34. Prep. HPLC 38% MeCN in water. <sup>1</sup>H NMR (MeCN-*d*<sub>3</sub>): δ 8.95 (br, 1H), 8.11 (s, 1H), 7.79 (s, 2H), 7.51 (d, *J* = 9.2 Hz, 1H), 7.32 (d, *J* = 8.8 Hz, 1H), 6.98 (m, 2H), 6.73 (d, *J* = 2.4 Hz, 1H), 6.62 (dd, *J* = 8.8 Hz, 2.4 Hz, 1H), 5.05 (m, 1H), 4.60 (m, 2H), 4.20 (m, 1H), 3.86 (m, 1H), 3.67 (m, 2H), 3.56 (m, 1H), 3.47 (m, 1H), 3.36 (m, 1H), 3.27 (m, 2H), 3.13 (m, 2H), 2.95 (m, 1H), 2.76 (m, 4H), 2.11 (m, 4H), 2.03 (m, 1H), 1.89 (m, 2H), 1.79 (m, 1H), 1.69 (m, 2H), 1.57 (m, 1H), 1.35 (m, 8H).

**2-Chloro-4-((3*S*)-8-(4-(4-((6-(2,6-dioxopiperidin-3-yl)-5,7-dioxo-3,5,6,7-tetrahydropyrrolo[3,4-*f*]isoindol-2(1*H*)-yl)piperidine-1-carbonyl)phenyl)-3-methyl-2,8-diazaspiro[4.5]decan-2-yl)benzonitrile (ARD-1671, 42).** UPLC–MS: 4.5 min, purity > 95%, MS [M + H]<sup>+</sup>; found, 774.29, calcd, 774.31. Prep. HPLC 38% MeCN in water. <sup>1</sup>H NMR (MeCN-*d*<sub>3</sub>): δ 8.97 (br, 1H), 7.85 (s, 2H), 7.70 (m, 2H), 7.53 (m, 3H), 6.79 (d, *J* = 2.4 Hz, 1H), 6.67 (dd, *J* = 8.8 Hz, 2.4 Hz, 1H), 5.05 (m, 1H), 4.92 (m, 2H), 4.59 (m, 2H), 4.09 (m, 2H), 3.63 (m, 3H), 3.45 (m, 6H), 2.98 (m, 3H), 2.76 (m, 5H), 2.39 (m, 2H), 2.04 (m, 4H), 1.75 (m, 1H), 1.21 (m, 3H).

**2-Chloro-4-((3*S*)-8-(4-(3-(6-(2,6-dioxopiperidin-3-yl)-5,7-dioxo-3,5,6,7-tetrahydropyrrolo[3,4-*f*]isoindol-2(1*H*)-yl)azetidine-1-carbonyl)phenyl)-3-methyl-2,8-diazaspiro[4.5]decan-2-yl)benzonitrile (ARD-1689, 43).** UPLC–MS: 4.5 min, purity > 95%, MS [M + H]<sup>+</sup>; found, 746.21, calcd, 746.28. Prep. HPLC 36% MeCN in water. <sup>1</sup>H NMR (MeCN-*d*<sub>3</sub>): δ 8.94 (br, 1H), 8.07 (m, 1H), 7.84 (m, 2H), 7.52 (dd, *J* = 10.4 Hz, 8.8 Hz, 2H), 7.01 (d, *J* = 9.2 Hz, 1H), 6.76

(d, *J* = 5.2 Hz, 1H), 6.64 (dd, *J* = 8.8 Hz, 2.0 Hz, 1H), 5.07 (m, 1H), 4.72 (m, 2H), 4.48 (m, 2H), 4.27 (m, 1H), 4.05 (m, 1H), 3.43 (m, 2H), 3.27 (m, 2H), 2.78 (m, 8H), 2.32 (m, 2H), 2.18 (m, 2H), 1.82 (m, 2H), 1.60 (m, 2H), 1.27 (m, 3H).

**2-Chloro-4-((3*S*)-8-(4-(3-((6-(2,6-dioxopiperidin-3-yl)-5,7-dioxo-3,5,6,7-tetrahydropyrrolo[3,4-*f*]isoindol-2(1*H*)-yl)methyl)azetidine-1-carbonyl)phenyl)-3-methyl-2,8-diazaspiro[4.5]decan-2-yl)benzonitrile (ARD-1690, 44).** UPLC–MS: 4.7 min, purity > 95%, MS [M + H]<sup>+</sup>; found, 760.23, calcd, 760.29. Prep. HPLC 39% MeCN in water. <sup>1</sup>H NMR (MeCN-*d*<sub>3</sub>): δ 8.95 (br, 1H), 7.86 (s, 2H), 7.60 (d, *J* = 8.8 Hz, 2H), 7.52 (d, *J* = 8.8 Hz, 1H), 7.05 (d, *J* = 9.2 Hz, 2H), 6.76 (d, *J* = 2.4 Hz, 1H), 6.62 (dd, *J* = 8.8 Hz, 2.4 Hz, 1H), 5.04 (m, 1H), 4.76 (m, 3H), 4.04 (m, 1H), 3.73 (m, 3H), 3.43 (m, 4H), 3.34 (m, 2H), 3.21 (m, 2H), 2.78 (m, 4H), 2.32 (m, 1H), 2.16 (m, 2H), 2.02 (m, 1H), 1.84 (m, 2H), 1.62 (m, 2H), 1.27 (m, 4H).

**2-Chloro-4-((3*S*)-8-(4-(4-((6-(2,6-dioxopiperidin-3-yl)-5,7-dioxo-3,5,6,7-tetrahydropyrrolo[3,4-*f*]isoindol-2(1*H*)-yl)methyl)-4-fluoropiperidine-1-carbonyl)phenyl)-3-methyl-2,8-diazaspiro[4.5]decan-2-yl)benzonitrile (ARD-1683, 45).** UPLC–MS: 5.1 min, purity > 95%, MS [M + H]<sup>+</sup>; found, 806.32, calcd, 806.32. Prep. HPLC 42% MeCN in water. <sup>1</sup>H NMR (MeCN-*d*<sub>3</sub>): δ 8.93 (br, 1H), 7.82 (s, 2H), 7.52 (d, *J* = 8.8 Hz, 1H), 7.39 (d, *J* = 8.8 Hz, 2H), 7.11 (d, *J* = 8.8 Hz, 2H), 6.76 (d, *J* = 2.4 Hz, 1H), 6.64 (dd, *J* = 8.8 Hz, 2.4 Hz, 1H), 5.06 (m, 1H), 4.76 (m, 3H), 4.06 (m, 2H), 3.61 (m, 3H), 3.43 (m, 4H), 3.29 (m, 4H), 2.77 (m, 4H), 2.35 (m, 1H), 2.15 (m, 2H), 2.06 (m, 3H), 1.88 (m, 3H), 1.79 (m, 1H), 1.64 (m, 2H), 1.21 (d, *J* = 6.0 Hz, 3H).

**2-Chloro-4-((3*S*)-8-(4-(4-((6-(2,6-dioxopiperidin-3-yl)-5,7-dioxo-3,5,6,7-tetrahydropyrrolo[3,4-*f*]isoindol-2(1*H*)-yl)methyl)-4-methoxypiperidine-1-carbonyl)phenyl)-3-methyl-2,8-diazaspiro[4.5]decan-2-yl)benzonitrile (ARD-1684, 46).** UPLC–MS: 4.9 min, purity > 95%, MS [M + H]<sup>+</sup>; found, 818.32, calcd, 818.34. Prep. HPLC 40% MeCN in water. <sup>1</sup>H NMR (MeCN-*d*<sub>3</sub>): δ 8.97 (br, 1H), 7.84 (s, 2H), 7.52 (d, *J* = 8.8 Hz, 1H), 7.40 (d, *J* = 8.8 Hz, 2H), 7.17 (d, *J* = 8.8 Hz, 2H), 6.77 (d, *J* = 2.4 Hz, 1H), 6.46 (dd, *J* = 8.8 Hz, 2.4 Hz, 1H), 5.07 (m, 1H), 4.88 (m, 3H), 4.07 (m, 2H), 3.59 (m, 2H), 3.43 (m, 7H), 3.32 (m, 6H), 2.79 (m, 4H), 2.32 (m, 1H), 2.17 (m, 1H), 1.91 (m, 2H), 1.68 (m, 5H), 1.41 (m, 1H), 1.28 (d, *J* = 6.0 Hz, 3H).

**2-Chloro-4-((3*S*)-8-(4-(4-((6-(2,6-dioxopiperidin-3-yl)-5,7-dioxo-3,5,6,7-tetrahydropyrrolo[3,4-*f*]isoindol-2(1*H*)-yl)methyl)-4-methylpiperidine-1-carbonyl)phenyl)-3-methyl-2,8-diazaspiro[4.5]decan-2-yl)benzonitrile (ARD-1694, 47).** UPLC–MS: 5.4 min, purity > 95%, MS [M + H]<sup>+</sup>; found, 802.30, calcd, 802.34. Prep. HPLC 43% MeCN in water. <sup>1</sup>H NMR (MeCN-*d*<sub>3</sub>): δ 8.95 (br, 1H), 7.82 (s, 2H), 7.52 (d, *J* = 8.8 Hz, 1H), 7.36 (d, *J* = 9.2 Hz, 2H), 7.04 (d, *J* = 8.8 Hz, 2H), 6.75 (d, *J* = 2.4 Hz, 1H), 6.42 (dd, *J* = 9.2 Hz, 2.4 Hz, 1H), 5.07 (m, 1H), 4.83 (m, 3H), 4.19 (m, 1H), 4.06 (m, 1H), 3.89 (m, 1H), 3.38 (m, 9H), 3.05 (m, 1H), 2.76 (m, 4H), 2.39 (m, 1H), 2.31 (m, 1H), 2.18 (m, 2H), 2.03 (m, 1H), 1.86 (m, 2H), 1.65 (m, 4H), 1.28 (m, 6H).

**2-Chloro-4-((3*S*)-8-(4-(4-((6-(2,6-dioxopiperidin-3-yl)-5,7-dioxo-3,5,6,7-tetrahydropyrrolo[3,4-*f*]isoindol-2(1*H*)-yl)methyl)-4-hydroxypiperidine-1-carbonyl)phenyl)-3-methyl-2,8-diazaspiro[4.5]decan-2-yl)benzonitrile (ARD-1705, 48).** UPLC–MS: 4.4 min, purity > 95%, MS [M + H]<sup>+</sup>; found, 804.33, calcd, 804.32. Prep. HPLC 36% MeCN in water. <sup>1</sup>H NMR (MeCN-*d*<sub>3</sub>): δ 8.10 (br, 1H), 7.83 (s, 1H), 7.57 (d, *J* = 8.8 Hz, 1H), 7.52 (d, *J* = 8.8 Hz, 1H), 7.33 (d, *J* = 8.8 Hz, 2H), 7.01 (d, *J* = 9.2 Hz, 2H), 6.76 (d, *J* = 2.4 Hz, 1H), 6.62 (dd, *J* = 9.2 Hz, 2.4 Hz, 1H), 4.97 (m, 1H), 4.05 (m, 2H), 3.89 (m, 2H), 3.81 (m, 2H), 3.44 (m, 4H), 3.26 (m, 2H), 3.06 (m, 2H), 2.72 (m, 2H), 2.13 (m, 2H), 2.03 (m, 2H), 1.90 (m, 1H), 1.83 (m, 3H), 1.72 (m, 4H), 1.62 (m, 2H), 1.45 (m, 2H), 1.28 (m, 3H).

**2-Chloro-4-((3*S*)-8-(6-(4-((6-(2,6-dioxopiperidin-3-yl)-5,7-dioxo-3,5,6,7-tetrahydropyrrolo[3,4-*f*]isoindol-2(1*H*)-yl)methyl)piperidine-1-carbonyl)pyridazin-3-yl)-3-methyl-2,8-diazaspiro[4.5]decan-2-yl)benzonitrile (ARD-7063, 49).** UPLC–MS: 4.2 min, purity > 95%, MS [M + H]<sup>+</sup>; found, 790.29, calcd, 790.32. Prep. HPLC 36% MeCN in water. <sup>1</sup>H NMR (MeCN-*d*<sub>3</sub>): δ 8.95 (br, 1H), 7.85 (s, 2H), 7.64 (d, *J* = 9.6 Hz, 1H), 7.53 (d, *J* = 8.8 Hz, 1H), 7.34 (d, *J* = 10.0 Hz, 1H), 6.76 (d, *J* = 2.4 Hz, 1H), 6.64 (dd, *J* = 8.8 Hz, 2.4 Hz, 1H), 5.05 (m, 2H), 4.97 (m, 3H), 4.63 (m, 1H), 4.16 (m, 1H), 4.05 (m, 1H), 3.87 (m, 2H), 3.67 (m, 2H), 3.43 (m, 2H), 3.33 (m, 2H), 3.18 (m, 1H), 2.91 (m, 1H), 2.72 (m, 3H), 2.33 (m, 1H), 2.24 (m, 1H), 2.14 (m, 1H), 2.05 (m,

1H), 1.89 (m, 1H), 1.79 (m, 2H), 1.66 (m, 1H), 1.59 (m, 1H), 1.42 (m, 3H), 1.28 (d,  $J = 6.4$  Hz, 3H).

**2-Chloro-4-((3S)-8-(5-(4-((6-(2,6-dioxopiperidin-3-yl)-5,7-dioxo-3,5,6,7-tetrahydropyrrolo[3,4-f]isoindol-2(1H)-yl)methyl)-piperidine-1-carbonyl)pyrazin-2-yl)-3-methyl-2,8-diazaspiro[4.5]-decan-2-yl)benzotrile (ARD-7064, 50).** UPLC–MS: 4.3 min, purity > 95%, MS  $[M + H]^+$ ; found, 790.28, calcd, 790.32. Prep. HPLC 41% MeCN in water.  $^1H$  NMR (MeCN- $d_3$ ):  $\delta$  8.95 (br, 1H), 8.64 (d,  $J = 0.8$  Hz, 1H), 8.10 (s, 1H), 7.85 (s, 2H), 7.53 (d,  $J = 8.8$  Hz, 1H), 6.76 (d,  $J = 3.2$  Hz, 1H), 6.64 (dd,  $J = 9.2$  Hz, 2.4 Hz, 1H), 5.05 (m, 2H), 4.97 (m, 3H), 4.63 (m, 1H), 4.16 (m, 1H), 4.05 (m, 1H), 3.87 (m, 2H), 3.67 (m, 2H), 3.43 (m, 2H), 3.33 (m, 2H), 3.18 (m, 1H), 2.91 (m, 1H), 2.72 (m, 3H), 2.33 (m, 1H), 2.24 (m, 1H), 2.14 (m, 1H), 2.05 (m, 1H), 1.89 (m, 1H), 1.79 (m, 2H), 1.66 (m, 1H), 1.59 (m, 1H), 1.42 (m, 3H), 1.28 (d,  $J = 6.4$  Hz, 3H).

**2-Chloro-4-((3S)-8-(6-(4-((6-(2,6-dioxopiperidin-3-yl)-5,7-dioxo-3,5,6,7-tetrahydropyrrolo[3,4-f]isoindol-2(1H)-yl)methyl)-piperidine-1-carbonyl)pyridin-3-yl)-3-methyl-2,8-diazaspiro[4.5]-decan-2-yl)benzotrile (ARD-4055, 51).** UPLC–MS: 4.2 min, purity > 95%, MS  $[M + H]^+$ ; found, 789.29, calcd, 789.32. Prep. HPLC 36% MeCN in water.  $^1H$  NMR (MeCN- $d_3$ ):  $\delta$  8.95 (br, 1H), 8.20 (d,  $J = 2.0$  Hz, 1H), 7.85 (s, 2H), 7.82 (dd,  $J = 9.2$  Hz, 2.4 Hz, 1H), 7.53 (d,  $J = 8.8$  Hz, 1H), 7.06 (d,  $J = 9.2$  Hz, 1H), 6.76 (d,  $J = 2.4$  Hz, 1H), 6.64 (dd,  $J = 8.8$  Hz, 2.4 Hz, 1H), 5.07 (m, 1H), 4.83 (m, 2H), 4.60 (m, 2H), 4.43 (m, 1H), 4.27 (m, 1H), 4.05 (m, 2H), 3.78 (m, 2H), 3.64 (m, 2H), 3.41 (m, 2H), 3.33 (m, 2H), 3.15 (m, 1H), 3.02 (m, 1H), 2.80 (m, 4H), 2.32 (m, 1H), 2.19 (m, 2H), 2.03 (m, 1H), 1.91 (m, 1H), 1.80 (m, 1H), 1.68 (m, 1H), 1.58 (m, 1H), 1.36 (m, 5H).

**2-Chloro-4-((3S)-8-(5-(4-((6-(2,6-dioxopiperidin-3-yl)-5,7-dioxo-3,5,6,7-tetrahydropyrrolo[3,4-f]isoindol-2(1H)-yl)methyl)-piperidine-1-carbonyl)pyridin-2-yl)-3-methyl-2,8-diazaspiro[4.5]-decan-2-yl)benzotrile (ARD-4056, 52).** UPLC–MS: 4.1 min, purity > 95%, MS  $[M + H]^+$ ; found, 789.33, calcd, 789.32. Prep. HPLC 36% MeCN in water.  $^1H$  NMR (MeCN- $d_3$ ):  $\delta$  8.97 (br, 1H), 8.29 (d,  $J = 2.8$  Hz, 1H), 7.84 (s, 2H), 7.56 (d,  $J = 8.8$  Hz, 1H), 7.50 (d,  $J = 8.8$  Hz, 2H), 6.75 (d,  $J = 2.4$  Hz, 1H), 6.64 (dd,  $J = 8.8$  Hz, 2.4 Hz, 1H), 5.90 (m, 4H), 5.02 (m, 1H), 4.83 (m, 4H), 4.04 (m, 1H), 3.45 (m, 2H), 3.34 (m, 5H), 3.10 (m, 2H), 2.78 (m, 3H), 2.31 (m, 1H), 2.17 (m, 2H), 1.91 (m, 1H), 1.82 (m, 2H), 1.65 (m, 3H), 1.42 (m, 2H), 1.26 (d, 3H).

**Computational Modeling of AR and Cereblon Ligands.** All modeling was conducted using the software package MOE.<sup>45</sup> The AR ligand-binding domain in complex with S-1 (PDB id: 2AXA) was utilized for conducting docking experiments to the AR.<sup>33</sup> The crystal structure obtained from the RCSB was first imported into MOE and prepared for modeling in a standard fashion. Crystallization additives and crystallographic water molecules were removed. Chain breaks if present due to unresolved residues were either capped or built in using MOE utilities. N- and C-termini were capped with ACE and NME. Missing side chains were built in using MOE utilities. Bond orders for crystallographic ligands were corrected if necessary. Hydrogen atoms were added, and the systems were parameterized using AMBER10<sup>46</sup> as implemented in the MOE package. At the time of this study, suitable structures for the AR in an open, antagonist conformation are not available. Ligands that are antagonists of the AR typically cannot fit into the closed conformation of the receptor. To create a *pseudo*-open conformation for the receptor for these docking studies, helix 12 of the AR was removed. Specifically, residues SER888 to LEU907 were removed and the ends of the resulting chain break were capped. All heavy atoms were fixed, and the positions of the hydrogen atoms were allowed to relax using energy minimization.

The DDB1: cereblon complex with lenalidomide (PDB id: 4CI2) was utilized for conducting docking experiments on cereblon.<sup>47</sup> The complex was prepared for modeling as described above. Once prepared, the DDB1 protein was removed.

Ligands to be docked were built into MOE; hydrogen atoms were added, charged with AMBER 10, and energy-minimized before docking. Docking was conducted using MOE's template docking method with substructure matching. The crystallographic ligand was used to define the binding site. The maximum common substructure between the crystallographic ligand and the ligand to be docked was used for the substructure matching. This method takes conformations

for the ligand to be docked and superimposes them into the protein binding site by aligning it to the substructure of the crystallographic ligand. Once aligned, the crystallographic ligand was removed, and additional conformational sampling of the ligand being docked was conducted. That sampling was followed by energy minimization of the docked ligand, keeping the protein rigid to create a refined pose which was then scored for ranking. To provide better substructure matching, the S-1 crystallographic ligand of 2AXA was modified by replacing the trifluoromethyl with chlorine and the nitro group with nitrile.

Default settings for MOE were used except that sampling was increased by increasing the number of placements for refinement, and the level of refinement was increased by changing the energy minimization termination criterion to a minimum value for the gradient and a maximum value for the number of iterations.

**AR Binding Assay.** A PolarScreen AR Competitor Assay Kit (Thermo Fisher, A15880) was used for the AR fluorescence polarization (FP) binding assay. In brief, the FP binding assay was performed in 384-well low-volume black round-bottom microplates (Corning, 4514) using the CLARIOstar microplate reader (BMG Labtech). To each well, 3.6 nM Fluormone AL Green and 400 nM AR-LBD protein were added to a final volume of 20  $\mu$ L in the assay buffer (AR green assay buffer with 2 mM DTT), with plates covered to protect reagents from light. The plate was incubated at room temperature for 4 h to reach equilibrium. The polarization values in millipolarization (mP) units were measured at an excitation wavelength of 485 nm and an emission wavelength of 530 nm. All experimental data were analyzed using Prism 8.0 software (GraphPad Software). IC<sub>50</sub> values were determined by nonlinear regression fitting of the competition curves (mP values vs log[compound]).

**Cell Lines and Cell Culture.** The LNCaP and VCaP human prostate cancer cell lines were purchased from the American Type Culture Collection (ATCC). LNCaP cells were grown in RPMI 1640 (Invitrogen), and VCaP cells were grown in DMEM with Glutamax (Invitrogen). Cells were supplemented with 10% fetal bovine serum (Invitrogen) at 37 °C in a humidified 5% CO<sub>2</sub> incubator. Cell viability was evaluated by a WST-8 assay (Dojindo) following the manufacturer's instructions. Western blot analysis was performed as previously described.<sup>16,17</sup>

**Quantitative Real-Time Polymerase Chain Reaction.** A real-time PCR was performed using QuantStudio 7 Flex Real-Time PCR System as described previously.<sup>16,17</sup> In brief, RNA was purified using the Qiagen RNase-Free DNase set; then, after quantification, the extracted RNA was converted to cDNA using a high-capacity RNA-to-cDNA kit from Applied Biosystems (Thermo Fisher Scientific). The levels of AR, TMPRSS2, FKBPS, PSA (KLK3), and GAPDH were quantified using TaqMan Fast Advanced Master Mix from Applied Biosystems. The level of gene expression was evaluated using the comparative CT method, which compares the CT value to GAPDH ( $\Delta$ CT) and then to vehicle control ( $\Delta\Delta$ CT).

**Microsomal Metabolic Stability Assay.** In vitro microsomal metabolic stability studies of AR degraders were performed in Medicilon Inc (Shanghai, China). The metabolic stability of a test compound was assessed using pooled mouse, rat, dog, monkey, and human liver microsomes, which were purchased from XenoTech (Lenexa, Kansas). In brief, the test compound (1  $\mu$ M) was incubated with the respective liver microsomes (0.5 mg/mL) and 1.7 mM cofactor-NADPH in 0.1 M K-phosphate buffer (pH = 7.4) containing 5 mM MgCl<sub>2</sub> at 37 °C, with the acetonitrile concentration less than 0.1% in the final incubation solution. After 0, 5, 10, 15, 30, and 45 min of incubation, the reaction was stopped immediately by adding 150  $\mu$ L of cold acetonitrile containing IS to each 45  $\mu$ L incubation solution in the wells of corresponding plates, respectively. The incubation without the addition of NADPH was used as the negative control. Ketanserin was used as the positive control. After quenching, the plate was shaken for 10 min (600 rpm) and centrifuged at 6000 rpm for 15 min. 80  $\mu$ L of the supernatant was then transferred from each well into a 96-well plate containing 140  $\mu$ L of water for LC–MS/MS analysis, from which the remaining amount of the test compound was determined. The natural log of the remaining amount of the test compound was plotted against

time to determine the disappearance rate and the half-life of the test compound.

**Hepatocyte Stability Assay.** Pooled mixed-gender cryopreserved human, monkey, mouse, rat, and dog hepatocytes were obtained from different commercial sources and stored in liquid nitrogen until use. Before experiments, the vial of cryopreserved hepatocytes was removed from the liquid nitrogen storage unit and thawed rapidly in a shaking water bath at 37 °C. The contents of each vial were poured into 40 mL of prewarmed (37 °C) William's Medium E (WME, pH 7.4) and gently mixed before centrifugation at 500 rpm for 5 min at room temperature. After centrifugation, the supernatant was discarded without disturbing the cell pellet. The cell was resuspended with preheated WME. Then, the hepatocyte cells were counted, and the cell suspension was diluted to the appropriate density (viable cell density =  $2 \times 10^6$  cells/mL). Viabilities for each hepatocyte experiment were at least 80%. The cell suspension was diluted in WME to give twice the incubation concentration and prewarmed at 37 °C for 15 min. A 4 mM spiking solution was made by adding 20  $\mu$ L of the substrate stock solution (10 mM) into 30  $\mu$ L of DMSO. 2  $\mu$ L of a 4 mM spiking solution was added to 3998  $\mu$ L of WME to make a 2 $\times$  dosing solution (2  $\mu$ M). To prepare for the testing, 40  $\mu$ L of the prewarmed hepatocyte solution ( $2 \times 10^6$  cells/mL) was added to the 48-well tissue culture-treated polystyrene incubation plate designated for different time points. Incubations (performed in duplicate) were initiated by the addition of 40  $\mu$ L of the prewarmed 2 $\times$  dosing solution to the wells designed for 5, 15, 30, 60, and 120 min and start timing (1  $\mu$ M final substrate concentration). The assay plate was placed in an incubator at 37 °C with 5% CO<sub>2</sub> and shaken at 110 rpm. For 0 min, 240  $\mu$ L of ACN containing IS was added to the wells of the 0 min plate, followed by addition of 40  $\mu$ L of the 2 $\times$  dosing solution. The plate was then sealed. For other time points, reactions were terminated at 5, 15, 30, 60, and 120 min by adding 240  $\mu$ L of ACN containing IS to the wells, respectively. The plate was sealed and stored at -35 °C in a freezer. After samples for all the time points were collected, the plate was shaken for 2 min and then centrifuged at 6000 rpm for 15 min. Finally, 100  $\mu$ L of the supernatant was transferred from each well into a clean 96-well sample plate containing 100  $\mu$ L of water for LC/MS analysis.

**Plasma Stability Assay.** The in vitro plasma stability of a test compound was studied in human, mouse, rat, dog, and monkey plasmas at Medicilon Inc. (Shanghai, China). Human plasma was purchased from ZenBio (Durham, NC, USA), and other plasmas were prepared in-house. A test compound was dissolved in DMSO to a final concentration of 10 mM and then diluted to 10  $\mu$ M in 0.1 M K/Mg buffer. 90  $\mu$ L of prewarmed plasma at 37 °C was added to the wells of a 96-well plate before spiking them with 10  $\mu$ L of the 10  $\mu$ M test compound to make the final concentration of the test compound of 1  $\mu$ M. The spiked plasma samples were incubated at 37 °C for 2 h. Reactions were terminated at 0, 5, 15, 30, 60, and 120 min by adding 400  $\mu$ L of acetonitrile containing IS. After quenching, the plates were shaken for 5 min at 600 rpm and stored at -20 °C if necessary, before analysis by LC/MS. Before LC/MS analysis, the samples were thawed at room temperature and centrifuged at 6000 rpm for 20 min. 100  $\mu$ L of the supernatant from each well was transferred into a 96-well sample plate containing 100  $\mu$ L of water for LC/MS analysis. Procaine was used as a reference control compound for human, mouse, dog, and monkey plasma stability studies, and benfluorex was used as a reference control compound for rat plasma stability studies. The in vitro plasma half-life ( $t_{1/2}$ ) was calculated using the expression  $t_{1/2} = 0.693/b$ , where  $b$  is the slope found in the linear fit of the natural logarithm of the fraction remaining of the test compound vs incubation time.

**CYP Inhibition Assay.** The CYP inhibition of a test compound was studied in human liver microsomes at Medicilon Inc. (Shanghai, China). In brief, a 0.2 mg/mL human liver microsomes stock solution was prepared by adding 10  $\mu$ L of 20 mg/mL microsomes to 990  $\mu$ L of 0.1 M KH<sub>2</sub>PO<sub>4</sub> (pH 7.4). In general, human liver microsomes were mixed with the buffer (0.1 M K-buffer), a test compound, or a reference inhibitor and warmed to 37 °C in a 96-well temperature-controlled heater block for 5 min. Aliquots of this mixture (30  $\mu$ L and in duplicate) were delivered to each well of a 96-well polypropylene polymerase chain reaction plate maintained at 37 °C, followed by adjoining of the

substrate (15  $\mu$ L) as applicable. The final organic solvent concentration was 1% (v/v) or less. Incubation was commenced with addition of the NADPH stock solution (15  $\mu$ L, 8 mM, pre-incubated at 37 °C) to a final incubation volume of 60  $\mu$ L and maintained at 37 °C for a period (5 min for 3A4, 10 min for 1A2, 2B6 and 2C9, 20 min for 2C8 and 2D6, and 45 min for 2C19). Incubations were typically terminated by adding 180  $\mu$ L of cold ACN containing IS. After quenching, the plates were shaken at the vibrator for 10 min (600 rpm) and then centrifuged at 6000 rpm for 15 min. 80  $\mu$ L of the supernatant was transferred from each well into a 96-well sample plate containing 120  $\mu$ L of ultrapure water for LC/MS analysis. Phenacetin, amfebutamone HCl, paclitaxel, diclofenac, *S*-mephenytoin, and dextromethorphan were used as substrates for CYP 1A2, 2B6, 2C8, 2C9, 2C19, and 2D6 isoforms, respectively, and midazolam and testosterone were used as substrates for CYP 3A4.  $\alpha$ -Naphthoflavon, ticlopidine, montelukast, sulfaphenazole, omeprazole, quinidine, and ketoconazole were used as reference inhibitor controls for CYP 1A2, 2B6, 2C8, 2C9, 2C19, 2D6, and 3A4, respectively.

**hERG Assay.** ARD-1676 was tested for its effect on hERG (human ether-à-go-go-related gene) potassium channels in a HEK 293 cell line stably expressed hERG using a manual patch-clamp technique.<sup>48</sup> In brief, ARD-1676 was tested at 3 and 30  $\mu$ M in duplicate, with terfenadine included as the positive control. ARD-1676 or the positive article was tested at room temperature using the whole-cell patch-clamp technique<sup>48</sup> with a PatchMaster patch-clamp system (HEKA Elektronik, Germany).

**PK Studies in Mice, Rats, Dogs, and Monkeys.** PK studies in mice, rats, dogs, and monkeys were performed at Medicilon, Inc. (Shanghai, China). Male ICR mice, male Sprague-Dawley (SD) rats, male beagle dogs, and male cynomolgus monkeys were used for PK studies, and each IV and oral arm consisted of three animals. For mouse PK studies, 10% PEG400 + 90% PBS (adjust pH to 8.0 by 0.5 N NaOH) was used as the formulation for both intravenous administration at 2 mg/kg and PO administration at 5 mg/kg. For rat PK studies, 10% PEG400 + 90% PBS (the pH was adjusted to 8.0 with 0.5 N NaOH) was used as the formulation for intravenous administration at 1 mg/kg and 5% DMSO + 10% solutol + 85% saline was used as the formulation for PO administration at 10 mg/kg. For dog PK studies of ARD-1676, 10% PEG400 + 90% PBS (the pH was adjusted to 8.0 with 0.5 N NaOH) as the formulation was used for intravenous administration at 1 mg/kg and 90% PEG400 + 10% cremophor as the formulation was used for PO administration at 3 mg/kg. For monkey PK studies of ARD-1676, 10% PEG400 + 90% PBS (the pH was adjusted to 8.0 with 0.5 N NaOH) was used as the formulation for intravenous administration at 1 mg/kg and 75% gelucire + 25% propylene glycol (pH = 7) as the formulation was used for PO administration at 3 mg/kg.

Animals were dosed with the testing compound ARD-1676 in its respective formulations, followed by collection of blood samples (100–200  $\mu$ L) from individual cohorts of animals ( $n = 3$ ) using heparinized calibrated pipettes or tubes (at 5 min, 15 min, 30 min, 1 h, 2 h, 4 h, 6 h, 8 h, and 24 h) and centrifuged at 6800g for 6 min at 2–8 °C. Subsequently, the resulting plasma was transferred to appropriately labeled tubes within 1 h of blood collection/centrifugation and stored frozen at -80 °C for analysis.

An aliquot of 20  $\mu$ L of plasma from each sample was protein-precipitated with 400  $\mu$ L of MeOH which contains 100 ng/mL IS. The mixture was vortexed for 1 min and centrifuged at 18,000g for 10 min. Then, 200  $\mu$ L of the supernatant was transferred to 96-well plates for LC-MS/MS analysis. To determine drug concentrations in plasma, a LC-MS/MS method was developed and validated for ARD-1676. The LC-MS/MS method consisted of an UPLC system, and chromatographic separation of ARD-1676 was achieved using a Waters ACQUITY UPLC BEH C18 1.7  $\mu$ m column (2.1  $\times$  50 mm). A Sciex QTrap 6500+ mass spectrometer equipped with an electrospray ionization source (Applied Biosystems, Toronto, Canada) in the positive-ion multiple reaction monitoring (MRM) mode was used for detection. The precursor/product ion transitions were monitored at  $m/z$  788.32–394.66 and 271.10–172.00 for ARD-1676 and IS tolbutamide, respectively, in the positive electrospray ionization

mode. The mobile phases used on UPLC were 0.1% formic acid in purified water (A) and 0.1% formic acid in acetonitrile (B). The gradient (B) was held at 10% (0–0.1 min), increased to 90% at 0.7 min, then stayed at isocratic 90% B for 0.4 min, and then immediately stepped back down to 10% for 0.3 min of re-equilibration. The flow rate was set at 0.6 mL/min. The column oven was set at 40 °C. An aliquot of 1  $\mu$ L of the supernatant was injected for LC–MS/MS analysis using an autosampler. The analytical results were confirmed using quality control samples for intra-assay variation. The accuracy of >66.7% of the quality control samples was between 80 and 120% of the known value(s). All pharmacokinetic parameters were calculated by non-compartmental methods using Phoenix WinNonlin, version 7.0 (Pharsight, USA).

**PK/PD and Efficacy Studies in Mice.** With the exception of PK studies in mice, rats, and dogs, all other in vivo studies were performed under animal protocols (PRO00011174 and PRO00009463) approved by the Institutional Animal Care and Use Committee (IACUC) of the University of Michigan, in accordance with the recommendations in the Guide for the Care and Use of Laboratory Animals of the National Institutes of Health.

To grow VCaP xenograft tumors, male CB17 SCID mice (Charles River Laboratories) were injected subcutaneously with  $5 \times 10^6$  VCaP cells (ATCC) in 5 mg/mL Matrigel (Corning).

For determination of oral exposures for AR degraders, each compound was administered in non-tumor-bearing male mice via oral gavage using 100% PEG200 as the dosing vehicle. Animals were sacrificed at indicated time points with 3 mice for each time point for each compound, and 300  $\mu$ L of blood was collected from each animal and stored at –80 °C until analysis.

For PK/PD studies in tumor-bearing male SCID mice, each compound was administered in animals via oral gavage using 100% PEG200 as the dosing vehicle when the VCaP tumors reached approximately 200 mm<sup>3</sup>. Animals were sacrificed at indicated time points with 3 mice for each compound at each time point, and blood (300  $\mu$ L) and tumors were collected from each animal for analysis. Isolated tumor samples were immediately frozen and ground with a mortar and pestle in liquid nitrogen. All plasma and tumor samples were stored at –80 °C until analysis. For analysis of AR protein levels in tumor samples, resected VCaP xenograft tumor tissues were ground into powder in liquid nitrogen and lysed in CST lysis buffer with halt proteinase inhibitors. Twenty micrograms of whole-tumor-clarified lysates were separated on 4–20 or 4–12% Novex gels. Western blots were performed as detailed in the previous section.

All PK/PD and efficacy animal experiments in this study were approved by the University of Michigan Committee on Use and Care of Animals and the Unit for Laboratory Animal Medicine (ULAM). The pharmacokinetics of ARD-1676 and analogues was determined in tumor-free female SCID mice or with VCaP tumor following oral gavage (PO) single dose at 10 or 20 mg/kg. The solid compounds were dissolved in a vehicle containing 100% PEG200. The animals (total 9 mice/compound or 6 mice/compound) were sacrificed at 1, 3, and 6 or 6 and 24 h after the final administration of the chemicals, followed by the collection of blood samples (300  $\mu$ L) and tumor samples. The blood samples were centrifuged at 15,000 rpm for 10 min, and then the supernatant plasma was saved for analysis. Isolated tumor samples were placed in a tube with ceramic beads (Precellys CK28-R) and immediately frozen in liquid nitrogen for PK analysis. All plasma and tumor samples were stored at –80 °C until analysis. To prepare tumor samples for LC–MS analysis, mixed ultrapure water and an ACN solution (4:1) were added to the defrosted tumor tissue samples 5:1, v/w, in order to facilitate homogenization with Precellys evolution homogenizer at 4 °C. The homogenized tissue solution was denatured using cold acetonitrile (1:3, v/v) with vortex and centrifuged at 13,000 rpm 4 °C for 10 min. Following protein precipitation, the final supernatants were collected for LC–MS analysis.

To determine drug concentrations in plasma and tumor samples, a LC–MS/MS method was developed and validated. The LC–MS/MS method consisted of a Shimadzu HPLC system, and chromatographic separation of a test compound was achieved using a Waters XBridge-C18 column (5 cm  $\times$  2.1 mm, 3.5  $\mu$ m). An AB Sciex QTrap 5500 mass

spectrometer equipped with an electrospray ionization source (Applied Biosystems, Toronto, Canada) in the positive-ion MRM mode was used for detection. The mobile phases used in HPLC were 0.1% formic acid in purified water (A) and 0.1% formic acid in acetonitrile (B). The gradient (B) was held at 10% (0–0.3 min), increased to 95% at 0.7 min, then stayed at isocratic 95% B for 2.3 min, and then immediately stepped back down to 10% for 2 min re-equilibration. The flow rate was set at 0.4 mL/min. All pharmacokinetic parameters were calculated by noncompartmental methods using WinNonlin, version 3.2 (Pharsight Corporation, Mountain View, CA, USA).

For the in vivo efficacy experiments, when VCaP tumors reached an average volume of 150 mm<sup>3</sup>, mice were tumor size-matched and randomly assigned to different experimental groups with 7 mice for each group. Drugs or vehicle control were given in the dosing schedule as indicated using 100% PEG200 as the dosing vehicle. Tumor sizes and animal weights were measured 2–3 times per week. Tumor volume (mm<sup>3</sup>) = (length  $\times$  width<sup>2</sup>)/2. Tumor growth inhibition was calculated as TGI (%) =  $(V_c - V_t)/(V_c - V_o) \times 100$ , where  $V_c$  and  $V_t$  are the medians of the control and treated groups at the end of the treatment, respectively, and  $V_o$  is that at the start. Tumor volumes at the end of treatment were statistically analyzed using a two-tailed, unpaired *t*-test (GraphPad Prism 8.0).

## ■ ASSOCIATED CONTENT

### Supporting Information

The Supporting Information is available free of charge at <https://pubs.acs.org/doi/10.1021/acs.jmedchem.3c01264>.

<sup>1</sup>H and <sup>13</sup>C NMR spectra for representative AR degraders and HPLC purity spectra for representative AR degraders (PDF)

Predicted binding models for ligand 23 (PDB)

Predicted binding models for ligand S-23a (PDB)

Predicted binding models for ligand 27 (PDB)

Predicted binding models for ligand 28 (PDB)

Predicted binding models for ligand 29 (PDB)

Molecular string file for all the final target compounds (CSV)

## ■ AUTHOR INFORMATION

### Corresponding Author

Shaomeng Wang – Department of Internal Medicine, Department of Pharmacology, Department of Medicinal Chemistry, Rogel Cancer Center, and Michigan Center for Translational Pathology, University of Michigan, Ann Arbor, Michigan 48109, United States; [orcid.org/0000-0002-8782-6950](https://orcid.org/0000-0002-8782-6950); Email: [Shaomeng@umich.edu](mailto:Shaomeng@umich.edu)

### Authors

Weiguo Xiang – Department of Internal Medicine, University of Michigan, Ann Arbor, Michigan 48109, United States

Lijie Zhao – Department of Internal Medicine, University of Michigan, Ann Arbor, Michigan 48109, United States

Xin Han – Department of Internal Medicine, University of Michigan, Ann Arbor, Michigan 48109, United States;

Present Address: Cancer Institute (Key Laboratory of Cancer Prevention and Intervention, China National Ministry of Education) of the 2nd Affiliated Hospital and Institute of Translational Medicine, Zhejiang University School of Medicine, Hangzhou 310029, China; State Key Laboratory for Chemistry and Molecular Engineering of Medicinal Resources (Guangxi Normal University)

Tianfeng Xu – Department of Internal Medicine, University of Michigan, Ann Arbor, Michigan 48109, United States;

Present Address: Department of Medicinal Chemistry, Shanghai Institute of Materia Medica, Chinese Academy of

Sciences, Shanghai 201203, China; University of Chinese Academy of Sciences, Beijing 100049, China; School of Pharmaceutical Science and Technology, Hangzhou Institute for Advanced Study, University of Chinese Academy of Sciences, Hangzhou 310024, China; [orcid.org/0000-0001-8996-4065](https://orcid.org/0000-0001-8996-4065)

**Steven Kregel** – Department of Pathology and Michigan Center for Translational Pathology, University of Michigan, Ann Arbor, Michigan 48109, United States; Present

Address: Department of Cancer Biology, Loyola University Chicago, Maywood, Illinois 60153, United States

**Mi Wang** – Department of Internal Medicine, University of Michigan, Ann Arbor, Michigan 48109, United States

**Bukeyan Miao** – Department of Internal Medicine, University of Michigan, Ann Arbor, Michigan 48109, United States

**Chong Qin** – Department of Internal Medicine, University of Michigan, Ann Arbor, Michigan 48109, United States;

Present Address: Key Laboratory of Marine Drugs, Chinese Ministry of Education, School of Medicine and Pharmacy, Ocean University of China, Qingdao, Shandong 266003, China; Center for Targeted Protein Degradation and Drug Discovery, Ocean University of China, Qingdao, Shandong 266003, China; Laboratory for Marine Drugs and Bioproducts, Pilot National Laboratory for Marine Science and Technology, Qingdao, Shandong 266137, China; [orcid.org/0000-0001-8108-1698](https://orcid.org/0000-0001-8108-1698)

**Mingliang Wang** – Department of Internal Medicine, University of Michigan, Ann Arbor, Michigan 48109, United States;

Present Address: Zhongshan Institute for Drug Discovery, Shanghai Institute of Materia Medica, Chinese Academy of Sciences, Zhongshan, China; Department of Medicinal Chemistry, Shanghai Institute of Materia Medica, Chinese Academy of Sciences, Shanghai, China

**Donna McEachern** – Department of Internal Medicine, University of Michigan, Ann Arbor, Michigan 48109, United States

**Jianfeng Lu** – Department of Internal Medicine, University of Michigan, Ann Arbor, Michigan 48109, United States

**Longchuan Bai** – Department of Internal Medicine and Rogel Cancer Center, University of Michigan, Ann Arbor, Michigan 48109, United States

**Chao-Yie Yang** – Department of Internal Medicine, University of Michigan, Ann Arbor, Michigan 48109, United States;

Present Address: Department of Pharmaceutical Sciences, College of Pharmacy, University of Tennessee Health Science Center, Memphis, Tennessee 38163, United States; [orcid.org/0000-0002-5445-0109](https://orcid.org/0000-0002-5445-0109)

**Paul D. Kirchhoff** – Department of Internal Medicine, University of Michigan, Ann Arbor, Michigan 48109, United States

**John Takyi-Williams** – Department of Pharmaceutical Sciences, University of Michigan, Ann Arbor, Michigan 48109, United States

**Lu Wang** – Department of Pharmaceutical Sciences, University of Michigan, Ann Arbor, Michigan 48109, United States

**Bo Wen** – Department of Pharmaceutical Sciences, University of Michigan, Ann Arbor, Michigan 48109, United States

**Duxin Sun** – Rogel Cancer Center and Department of Pharmaceutical Sciences, University of Michigan, Ann Arbor, Michigan 48109, United States; [orcid.org/0000-0002-6406-2126](https://orcid.org/0000-0002-6406-2126)

**Mark Ator** – Oncopia Therapeutics Inc, Malvern, Pennsylvania 19355, United States

**Robert Mckean** – Oncopia Therapeutics Inc, Malvern, Pennsylvania 19355, United States

**Arul M. Chinnaiyan** – Department of Pathology, Michigan Center for Translational Pathology, Rogel Cancer Center, and Howard Hughes Medical Institute, University of Michigan, Ann Arbor, Michigan 48109, United States

Complete contact information is available at:

<https://pubs.acs.org/10.1021/acs.jmedchem.3c01264>

### Author Contributions

♦W.X., L.Z., X.H., T.X., S.K., and M.W. contributed equally.

### Notes

The authors declare the following competing financial interest(s): The University of Michigan has filed patent applications on these AR degraders, which have been licensed to Oncopia Therapeutics, Inc. S. Wang, X. Han, L. Zhao, and W. Xiang are co-inventors on these patent applications and receive royalties from the University of Michigan. S. Wang was a co-founder of Oncopia Therapeutics and a paid consultant to Oncopia Therapeutics. S. Wang and the University of Michigan also owned equity in Oncopia, which was acquired by Roivant Science. S. Wang is a paid consultant to Roivant Sciences and Proteovant Therapeutics and owns equity in Roivant Sciences. The University of Michigan has received a research contract from Proteovant Therapeutics, Inc. and Oncopia Therapeutics (acquired by Proteovant) for which S. Wang serves as the principal investigator.

### ACKNOWLEDGMENTS

This study was supported in part by funding from Oncopia Therapeutics Inc., Proteovant Therapeutics Inc., the National Cancer Institute/NIH (P50 CA186786), and the University of Michigan Comprehensive Cancer Center Core Grant from the National Cancer Institute, NIH (P30CA046592).

### ABBREVIATIONS

ATCC, American Type Culture Collection; AR, androgen receptor; AUC<sub>0–24h</sub>, area under the curve between 0 and 24 h; C<sub>max</sub>, maximum drug concentration; Cl, plasma clearance rate; CYP, cytochrome P450; F, oral bioavailability; IACUC, Institutional Animal Care and Use Committee; IV, intravenous administration; MS, mass spectrometry; MRM, multiple reaction monitoring; PCa, prostate cancer; PROTAC, proteolysis-targeting chimera; PK, pharmacokinetics; PO, oral administration; PD, pharmacodynamics; qRT-PCR, quantitative real-time polymerase chain reaction; SD, standard deviation; SCID, severe combined immunodeficiency; SNIPERs, specific and nongenetic IAP-dependent protein erasers; T<sub>1/2</sub>, terminal half-life; TMS, tetramethylsilane; ULAM, Unit for Laboratory Animal Medicine; V<sub>ss</sub>, steady-state volume of distribution

### REFERENCES

- (1) Formaggio, N.; Rubin, M. A.; Theurillat, J.-P. Loss and Revival of Androgen Receptor Signaling in Advanced Prostate Cancer. *Oncogene* **2021**, *40*, 1205–1216.
- (2) Kobayashi, T.; Inoue, T.; Kamba, T.; Ogawa, O. Experimental Evidence of Persistent Androgen-Receptor-Dependency in Castration-Resistant Prostate Cancer. *Int. J. Mol. Sci.* **2013**, *14*, 15615–15635.
- (3) Saad, F.; Bögemann, M.; Suzuki, K.; Shore, N. Treatment of Nonmetastatic Castration-resistant Prostate Cancer: Focus on Second-generation Androgen Receptor Inhibitors. *Prostate Cancer Prostatic Dis.* **2021**, *24*, 323–334.

- (4) Chen, Y.; Zhou, Q.; Hankey, W.; Fang, X.; Yuan, F. Second Generation Androgen Receptor Antagonists and Challenges in Prostate Cancer Treatment. *Cell Death Dis.* **2022**, *13*, 632.
- (5) Watson, P. A.; Arora, V. K.; Sawyers, C. L. Emerging mechanisms of resistance to androgen receptor inhibitors in prostate cancer. *Nat. Rev. Cancer* **2015**, *15*, 701–711.
- (6) Salami, J.; Alabi, S.; Willard, R. R.; Vitale, N. J.; Wang, J.; Dong, H.; Jin, M.; McDonnell, D. P.; Crew, A. P.; Neklesa, T. K.; Crews, C. M. Androgen Receptor Degradation by the Proteolysis-Targeting Chimera ARCC-4 Outperforms Enzalutamide in Cellular Models of Prostate Cancer Drug Resistance. *Commun. Biol.* **2018**, *1*, 100.
- (7) Hwang, D.-J.; He, Y.; Ponnusamy, S.; Mohler, M. L.; Thiyagarajan, T.; McEwan, I. J.; Narayanan, R.; Miller, D. D. New Generation of Selective Androgen Receptor Degradators: Our Initial Design, Synthesis, and Biological Evaluation of New Compounds with Enzalutamide-Resistant Prostate Cancer Activity. *J. Med. Chem.* **2019**, *62*, 491–511.
- (8) Winter, G. E.; Buckley, D. L.; Paulk, J.; Roberts, J. M.; Souza, A.; Dhe-Paganon, S.; Bradner, J. E. Phthalimide conjugation as a strategy for in vivo target protein degradation. *Science* **2015**, *348*, 1376–1381 Drug Development.
- (9) Schneckloth, A. R.; Pucheault, M.; Tae, H. S.; Crews, C. M. Targeted Intracellular Protein Degradation Induced by a Small Molecule: En Route to Chemical Proteomics. *Bioorg. Med. Chem. Lett.* **2008**, *18*, 5904–5908.
- (10) Xiang, W.; Han, X.; Zhao, L.; Wang, S. Recent Advances in Targeting the Androgen Receptor with Protacs. *Med. Chem. Rev.* **2022**, *57*, 295–317.
- (11) Shibata, N.; Nagai, K.; Morita, Y.; Ujikawa, O.; Ohoka, N.; Hattori, T.; Koyama, R.; Sano, O.; Imaeda, Y.; Nara, H.; Cho, N.; Naito, M. Development of Protein Degradation Inducers of Androgen Receptor by Conjugation of Androgen Receptor Ligands and Inhibitor of Apoptosis Protein Ligands. *J. Med. Chem.* **2018**, *61*, 543–575.
- (12) Han, X.; Wang, C.; Qin, C.; Xiang, W.; Fernandez-Salas, E.; Yang, C.-Y.; Wang, M.; Zhao, L.; Xu, T.; Chinnaswamy, K.; Delproposto, J.; Stuckey, J.; Wang, S. Discovery of ARD-69 as a Highly Potent Proteolysis Targeting Chimera (PROTAC) Degradator of Androgen Receptor (AR) for the Treatment of Prostate Cancer. *J. Med. Chem.* **2019**, *62*, 941–964.
- (13) Han, X.; Zhao, L.; Xiang, W.; Qin, C.; Miao, B.; Xu, T.; Wang, M.; Yang, C.-Y.; Chinnaswamy, K.; Stuckey, J.; Wang, S. Discovery of Highly Potent and Efficient PROTAC Degradators of Androgen Receptor (AR) by Employing Weak Binding Affinity VHL E3 Ligase Ligands. *J. Med. Chem.* **2019**, *62*, 11218–11231.
- (14) Snyder, L. B.; Neklesa, T. K.; Chen, X.; Dong, H.; Ferraro, C.; Gordon, D. A.; Macaluso, J.; Pizzano, J.; Wang, J.; Willard, R. R.; Vitale, N.; Peck, R.; Moore, M. D.; Crews, C. M.; Houston, J.; Crew, A. P.; Taylor, I. Abstract 43: Discovery of ARV-110, a First in Class Androgen Receptor Degrading PROTAC for the Treatment of Men with Metastatic Castration Resistant Prostate Cancer. *Cancer Res.* **2021**, *81*, 43.
- (15) Dong, H.; Snyder, L. B.; Wang, J. Compounds and Methods for the Targeted Degradation of Androgen Receptor and Associated Methods of Use. U.S. Patent 20,220,144,809 A1, 2022.
- (16) Han, X.; Zhao, L.; Xiang, W.; Qin, C.; Miao, B.; McEachern, D.; Wang, Y.; Metwally, H.; Wang, L.; Matvekas, A.; Wen, B.; Sun, D.; Wang, S. Strategies toward Discovery of Potent and Orally Bioavailable Proteolysis Targeting Chimera Degradators of Androgen Receptor for the Treatment of Prostate Cancer. *J. Med. Chem.* **2021**, *64*, 12831–12854.
- (17) Xiang, W.; Zhao, L.; Han, X.; Qin, C.; Miao, B.; McEachern, D.; Wang, Y.; Metwally, H.; Kirchhoff, P. D.; Wang, L.; Matvekas, A.; He, M.; Wen, B.; Sun, D.; Wang, S. Discovery of ARD-2585 as an Exceptionally Potent and Orally Active PROTAC Degradator of Androgen Receptor for the Treatment of Advanced Prostate Cancer. *J. Med. Chem.* **2021**, *64*, 13487–13509.
- (18) Han, X.; Zhao, L.; Xiang, W.; Miao, B.; Qin, C.; Wang, M.; Xu, T.; McEachern, D.; Lu, J.; Wang, Y.; Metwally, H.; Yang, C.-Y.; Kirchhoff, P. D.; Wang, L.; Matvekas, A.; Takyi-Williams, J.; Wen, B.; Sun, D.; Ator, M.; McKean, R.; Wang, S. Discovery of ARD-2051 as a Potent and Orally Efficacious Proteolysis Targeting Chimera (PROTAC) Degradator of Androgen Receptor for the Treatment of Advanced Prostate Cancer. *J. Med. Chem.* **2023**, *66*, 8822–8843.
- (19) Petrylak, D. P.; Stewart, T. F.; Gao, X.; Berghorn, E.; Lu, H.; Chan, E.; Gedrich, R.; Lang, J. M.; McKean, M. A Phase 2 Expansion Study of ARV-766, a PROTAC Androgen Receptor (AR) Degradator, in Metastatic Castration-resistant Prostate Cancer (mCRPC). *J. Clin. Oncol.* **2023**, *41*, TPS290.
- (20) PROTAC Shrinks Mutated Prostate Tumors. *Cancer Discovery* **2022**, *12* (), OF2. DOI: 10.1158/2159-8290.CD-NB2022-0020.
- (21) Alexander, M. D.; Correa, M. D.; Dalvie, D.; Grant, V. H. S.; Hansen, J.; Harris, R. L., III; Horn, E. J.; Huang, D.; Mayne, C.; Norris, S.; Plantevin-Krenitsky, V.; Sapienza, J. J.; Tehrani, L.; Whitefield, B. W. Cereblon binding compounds, compositions thereof, and methods of treatment therewith. WO 2022272074 A1, 2022.
- (22) Alexander, M. D.; Correa, M. D.; Dalvie, D.; Grant, V. H. S.; Hansen, J.; Harris, R. L., III; Horn, E. J.; Huang, D.; Mayne, C.; Norris, S.; Plantevin-Krenitsky, V.; Sapienza, J. J.; Tehrani, L.; Whitefield, B. W. Cereblon binding compounds, compositions thereof, and methods of treatment therewith. WO 2021262815 A1, 2021.
- (23) Alexander, M. D.; Correa, M. D.; Dalvie, D.; Grant, V. H. S.; Hansen, J.; Harris, R. L., III; Horn, E. J.; Huang, D.; Mayne, C.; Norris, S.; Plantevin-Krenitsky, V.; Sapienza, J. J.; Tehrani, L.; Whitefield, B. W. Cereblon binding compounds, compositions thereof, and methods of treatment therewith. WO 2021262812 A1, 2021.
- (24) Alexander, M. D.; Correa, M. D.; Dalvie, D.; Grant, V. H. S.; Hansen, J.; Harris, R. L., III; Horn, E. J.; Huang, D.; Mayne, C.; Norris, S.; Plantevin-Krenitsky, V.; Sapienza, J. J.; Tehrani, L.; Whitefield, B. W. Cereblon binding compounds, compositions thereof, and methods of treatment therewith. WO 2021262810 A1, 2021.
- (25) Du, W.; Geng, X.; Wen, K.; Ai, C.; Lv, H.; Tu, Z.; Li, X.; Chen, Y. The purposes of a kind of benzo-heterocycle compound and its treating cancer. CN 109081813 A, 2018.
- (26) Du, W.; Li, X.; Wen, K.; Qin, D.; Zhang, S.; Chen, S.; Duan, J.; Lv, H.; Li, H.; Li, Y.; He, J.; Chen, M.; Liu, S.; Fu, Y.; Guan, Y.; Tu, Z. Bifunctional Chimeric Heterocyclic Compound and Use Thereof as Androgen Receptor Degradator. WO 2023006097 A1, 2023.
- (27) Du, W.; Wen, K.; Fu, Y.; Lv, H.; He, J.; Qin, D.; Li, Y.; Duan, J.; Li, Y.; Ai, C.; Tu, Z.; Chen, Y.; Li, X. A Class of Bifunctional Chimeric Heterocyclic Compounds for Targeted Degradation of Androgen Receptors and Application. WO 2020211822 A1, 2020.
- (28) Fan, J.; He, W.; Liu, K. Novel compounds having bet, estrogen receptor, and androgen receptor degradation activity and uses thereof. WO 2020214952 A1, 2020.
- (29) Fan, J.; Qian, Y.; He, W.; Liu, K. Substituted quinoline-8-carbonitrile derivatives having androgen receptor degradation activity and uses thereof. U.S. Patent 10,836,749 B1, 2020.
- (30) Fan, J.; Qian, Y.; He, W.; Liu, K. Preparation of Novel Ureas having Androgen Receptor Degradation Dctivity and Uses Thereof. U.S. Patent 20,210,087,170 A1, 2021.
- (31) Fan, J.; Qian, Y.; He, W.; Liu, K. Preparation of Novel Substituted Quinoline-8-carbonitrile Derivatives with Androgen Receptor Degradation Activity and Uses Thereof. U.S. Patent 20,210,087,171 A1, 2021.
- (32) Xiang, W.; Wang, S. Therapeutic Strategies to Target the Androgen Receptor. *J. Med. Chem.* **2022**, *65*, 8772–8797.
- (33) Bohl, C. E.; Miller, D. D.; Chen, J.; Bell, C. E.; Dalton, J. T. Structural Basis for Accommodation of Nonsteroidal Ligands in the Androgen Receptor. *J. Biol. Chem.* **2005**, *280*, 37747–37754.
- (34) Levinson, D. J.; Decker, D. E. Characterization of a [3H]-methyltrienolone (R1881) Binding Protein in Rat Liver Cytosol. *J. Steroid Biochem.* **1985**, *22*, 211–219.
- (35) Robinson, D.; Van Allen, E.; Wu, Y. M.; Schultz, N.; Lonigro, R. J.; Mosquera, J. M.; Montgomery, B.; Taplin, M. E.; Pritchard, C. C.; Attard, G.; Beltran, H.; Abida, W.; Bradley, R. K.; Vinson, J.; Cao, X.; Vats, P.; Kunju, L. P.; Hussain, M.; Feng, F. Y.; Tomlins, S. A.; Cooney, K. A.; Smith, D. C.; Brennan, C.; Siddiqui, J.; Mehra, R.; Chen, Y.; Rathkopf, D. E.; Morris, M. J.; Solomon, S. B.; Durack, J. C.; Reuter, V. E.; Gopalan, A.; Gao, J.; Loda, M.; Lis, R. T.; Bowden, M.; Balk, S. P.; Gaviola, G.; Sougnez, C.; Gupta, M.; Yu, E. Y.; Mostaghel, E. A.; Cheng, H. H.; Gulcahy, H.; True, L. D.; Plymate, S. R.; Dvinge, H.;

Ferraldeschi, R.; Flohr, P.; Miranda, S.; Zafeiriou, Z.; Tunariu, N.; Mateo, J.; Perez-Lopez, R.; Demichelis, F.; Robinson, B. D.; Schiffman, M.; Nanus, D. M.; Tagawa, S. T.; Sigaras, A.; Eng, K. W.; Elemento, O.; Sboner, A.; Heath, E. I.; Scher, H. I.; Pienta, K. J.; Kantoff, P.; de Bono, J.; Rubin, M. A.; Nelson, P. S.; Garraway, L. A.; Sawyers, C. L.; Chinnaiyan, A. M. Integrative clinical genomics of advanced prostate cancer. *Cell* **2015**, *161*, 1215–1228.

(36) Poukka, H.; Karvonen, U.; Janne, O. A.; Palvimo, J. J. Covalent modification of the androgen receptor by small ubiquitin-like modifier 1 (SUMO-1). *Proc. Natl. Acad. Sci. U.S.A.* **2000**, *97*, 14145–14150.

(37) Lalous, N.; Volik, S. V.; Awrey, S.; Leblanc, E.; Tse, R.; Murillo, J.; Singh, K.; Azad, A. A.; Wyatt, A. W.; LeBihan, S.; Chi, K. N.; Gleave, M. E.; Rennie, P. S.; Collins, C. C.; Cherkasov, A. Functional analysis of androgen receptor mutations that confer anti-androgen resistance identified in circulating cell-free DNA from prostate cancer patients. *Genome Biol.* **2016**, *17*, 10.

(38) Shiota, M.; Akamatsu, S.; Tsukahara, S.; Nagakawa, S.; Matsumoto, T.; Eto, M. Androgen receptor mutations for precision medicine in prostate cancer. *Endocr.-Relat. Cancer* **2022**, *29*, R143–R155.

(39) Balbas, M. D.; Evans, M. J.; Hosfield, D. J.; Wongvipat, J.; Arora, V. K.; Watson, P. A.; Chen, Y.; Greene, G. L.; Shen, Y.; Sawyers, C. L. Overcoming mutation-based resistance to antiandrogens with rational drug design. *Elife* **2013**, *2*, No. e00499.

(40) Shibata, T.; Otomo, M.; Tahara, Y.-k.; Endo, K. Highly diastereo- and Enantioselective Construction of Both Central and Axial Chiralities by Rh-catalyzed [2 + 2 + 2] Cycloaddition. *Org. Biomol. Chem.* **2008**, *6*, 4296–4298.

(41) Brun, S.; Parera, M.; Pla-Quintana, A.; Roglans, A.; León, T.; Achard, T.; Solà, J.; Verdager, X.; Riera, A. Chiral N-Phosphino Sulfinamide Ligands in Rhodium(I)-Catalyzed [2+2+2] Cycloaddition Reactions. *Tetrahedron* **2010**, *66*, 9032–9040.

(42) Cho, C. S.; Patel, D. B. A New Route for Isoquinolines Catalyzed by Palladium. *J. Mol. Catal. A: Chem.* **2006**, *260*, 105–108.

(43) Wang, S.; Xu, T.; Wang, M.; Hu, J.; Han, X.; Xiang, W.; Rej, R. Cereblon e3 ligase inhibitors. WO 2021041664 A1, 2021.

(44) Smith, A. C.; Cabral, S.; Kung, D. W.; Rose, C. R.; Southers, J. A.; Garcia-Irizarry, C. N.; Damon, D. B.; Bagley, S. W.; Griffith, D. A. The Synthesis of Methyl-Substituted Spirocyclic Piperidine-Azetidine (2,7-Diazaspiro[3.5]nonane) and Spirocyclic Piperidine-Pyrrolidine (2,8-Diazaspiro[4.5]decane) Ring Systems. *J. Org. Chem.* **2016**, *81*, 3509–3519.

(45) *Molecular Operating Environment (MOE)*; Chemical Computing Group ULC: 1010 Sherbrooke St. West, Suite #910, Montreal, QC, Canada, H3A 2R7, 2020.

(46) Case, D. A.; Darden, T. A.; Cheatham, T. E.; Simmerling, C. L.; Wang, J.; Duke, R. E.; Luo, R.; Crowley, M.; Walker, R. C.; Zhang, W.; Merz, K. M.; Wang, B.; Hayik, S.; Roitberg, A.; Seabra, G.; Kolossvary, I.; Wong, K. F.; Paesani, F.; Vanicek, J.; Wu, X.; Brozell, S. R.; Steinbrecher, T.; Gohlke, H.; Yang, L.; Tan, C.; Mongan, J.; Hornak, V.; Cui, G.; Mathews, D. H.; Seetin, M. G.; Sagui, C.; Babin, V.; Kollman, P. A. *Amber 10*; University of California: San Francisco, 2008.

(47) Fischer, E. S.; Böhm, K.; Lydeard, J. R.; Yang, H.; Stadler, M. B.; Cavadini, S.; Nagel, J.; Serluca, F.; Acker, V.; Lingaraju, G. M.; Tichkule, R. B.; Schebesta, M.; Forrester, W. C.; Schirle, M.; Hassiepen, U.; Ottl, J.; Hild, M.; Beckwith, R. E. J.; Harper, J. W.; Jenkins, J. L.; Thomä, N. H. Structure of the DDB1–CRBN E3 ubiquitin ligase in complex with thalidomide. *Nature* **2014**, *512*, 49–53.

(48) Chen, X. L.; Kang, J. S.; Rampe, D. Manual Whole-Cell Patch-Clamping of the HERG Cardiac K<sup>+</sup> Channel. *Methods Mol. Biol.* **2011**, *691*, 151–163.